



Published in final edited form as:

Cell Rep. 2021 October 19; 37(3): 109842. doi:10.1016/j.celrep.2021.109842.

Crim1 and Kelch-like 14 exert complementary dual-directional developmental control over segmentally specific corticospinal axon projection targeting

Vibhu Sahni^{1,2,3}, Yasuhiro Itoh¹, Sara J. Shnider^{1,4}, Jeffrey D. Macklis^{1,5,*}

¹Department of Stem Cell and Regenerative Biology, and Center for Brain Science, Harvard University, Cambridge, MA 02138, USA

²Present address: Burke Neurological Institute, White Plains, NY 10605, USA

³Feil Family Brain and Mind Research Institute, Weill Cornell Medicine, New York, NY 10065, USA

⁴Present address: Teva Pharmaceuticals, Netanya 4250483, Israel

⁵Lead contact

SUMMARY

The cerebral cortex executes highly skilled movement, necessitating that it connects accurately with specific brainstem and spinal motor circuitry. Corticospinal neurons (CSN) must correctly target specific spinal segments, but the basis for this targeting remains unknown. In the accompanying report, we show that segmentally distinct CSN subpopulations are molecularly distinct from early development, identifying candidate molecular controls over segmentally specific axon targeting. Here, we functionally investigate two of these candidate molecular controls, Crim1 and Kelch-like 14 (Klhl14), identifying their critical roles in directing CSN axons to appropriate spinal segmental levels in the white matter prior to axon collateralization. Crim1 and Klhl14 are specifically expressed by distinct CSN subpopulations and regulate their differential white matter projection targeting—Crim1 directs thoracolumbar axon extension, while Klhl14 limits axon extension to bulbar-cervical segments. These molecular regulators of descending spinal projections constitute the first stages of a dual-directional set of complementary controls over CSN diversity for segmentally and functionally distinct circuitry.

Graphical Abstract

This is an open access article under the CC BY-NC-ND license.

*Correspondence: jeffrey_macklis@harvard.edu.

AUTHOR CONTRIBUTIONS

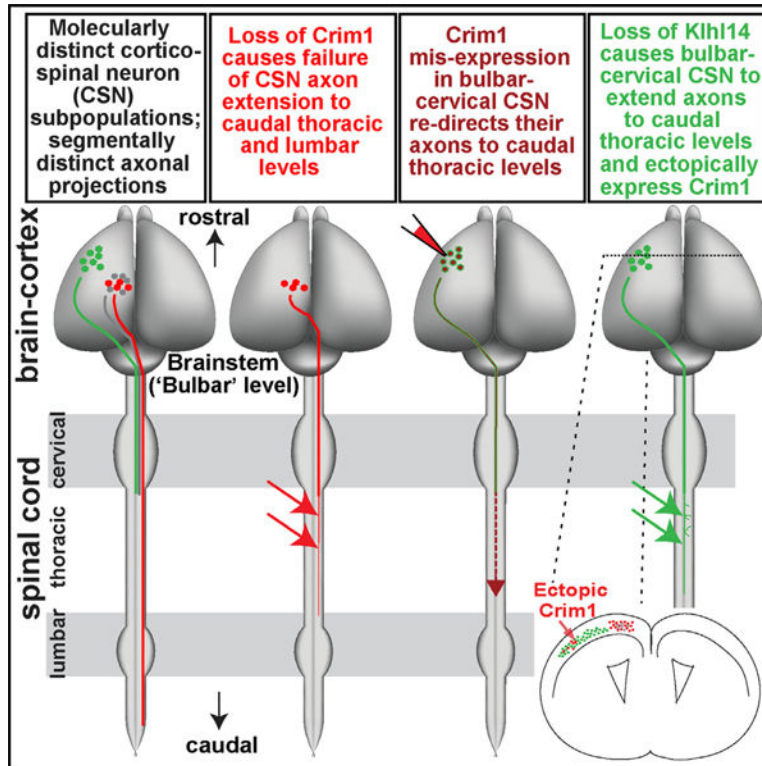
Research designed by V.S. and J.D.M.; performed by V.S., Y.I., and S.J.S.; data analyzed by V.S., Y.I., and J.D.M.; and manuscript written by V.S. and J.D.M.

SUPPLEMENTAL INFORMATION

Supplemental information can be found online at <https://doi.org/10.1016/j.celrep.2021.109842>.

DECLARATION OF INTERESTS

The authors declare no competing interests.



In brief

Corticospinal neurons (CSN) projecting axons to distinct spinal segments are molecularly distinct from early development. Sahni et al. show that a subset of these distinct molecules direct CSN axons to appropriate spinal levels: Crim1, a transmembrane protein, regulates thoracolumbar axon extension, while Kelch-like 14 (Kihl14) regulates bulbar-cervical extension.

INTRODUCTION

The corticospinal system is the principal spinal-projecting pathway controlling performance of highly skilled and complex movements (Martin, 2005). In addition, the corticospinal circuit exerts critical control over sensory modulation and autonomic functions (Lemon, 2008; Lemon and Griffiths, 2005; Liu et al., 2018; Sahni et al., 2020; Welniarz et al., 2017). For this precise top-down sensorimotor and autonomic control, distinct corticospinal neurons (CSN) extend axons to, and innervate, distinct subcerebral targets: rostral targets in the brainstem and cervical cord to caudal targets in the thoracic and lumbar cord. The molecular basis for this segmentally specific connectivity remains unknown.

Multiple investigations in mature CSN circuitry have aimed at understanding this diversity to elucidate functional diversity of cortical control over movement (e.g., CSN projecting to cervical cord broadly control arm and finger movement, while CSN projecting to lumbar cord broadly control leg movement). The somatotopic organization of adult cortex, wherein cortical regions are systematically organized to control movement of distinct body parts, has been well documented in the field, including in humans (Penfield and Boldrey, 1937;

Penfield and Rasmussen, 1950), non-human primates (Woolsey et al., 1952), and rodents (Akintunde and Buxton, 1992; Li et al., 1990; Miller, 1987; Tennant et al., 2011; Ullan and Artieda, 1981; Wise et al., 1979; Donoghue and Wise, 1982; Neafsey et al., 1986).

Rodent studies have identified that CSN residing in distinct cortical locations, including outside primary motor cortex (M1), exhibit distinct spinal connectivity (Ueno et al., 2018; Tennant et al., 2011; Wang et al., 2017). The cortical area extending projections to lumbar cord is significantly smaller than cortical areas originating corticospinal projections to cervical cord (Kamiyama et al., 2015; Wang et al., 2018). Understanding how corticospinal outputs target specific spinal segments is a major goal toward identifying the developmental basis for the organization of descending neocortical control over distinct, segmentally specific, function—including motor control, sensory modulation, and autonomic control.

Transcriptional regulators have been identified as controlling the identity of broad neocortical projection neuron subtypes (Fame et al., 2011; Franco and Müller, 2013; Greig et al., 2013; Leone et al., 2008; Lodato et al., 2015; Molyneaux et al., 2007). In particular, specification and differentiation of CSN is regulated first by controls over broad corticofugal projection neuron differentiation, then by controls over all subcerebral projection neurons, and then by CSN-subtype-specific molecular controls (Arlotta et al., 2005; Cederquist et al., 2013; Chen et al., 2005a, 2005b; Galazo et al., 2016; Greig et al., 2016; Han et al., 2011; Joshi et al., 2008; Kwan et al., 2008; Lai et al., 2008; Lodato et al., 2014; McKenna et al., 2011; Molyneaux et al., 2005; Ozdinler and Macklis, 2006; Shim et al., 2012; Tomassy et al., 2010; Woodworth et al., 2012, 2016). Guidance molecules direct CSN axons at specific choice points, including in the spinal cord (e.g., EphA4; reviewed by Canty and Murphy 2008; Sahni et al. 2020; Welniarz et al. 2017). Further, specific signaling mechanisms promote CSN axon extension into the cord (e.g., insulin growth factor [IGF]-I [Ozdinler and Macklis, 2006] and Wnt-Ryk signaling [Liu et al., 2005]). However, all these mechanisms, including CSN-specific molecular controls identified to date, do not distinguish between hodologically distinct CSN subpopulations, and the molecular basis for the segmentally specific CSN connectivity described above remains entirely unknown.

In the accompanying study (Sahni et al., 2021), we identify that developing CSN subpopulations exhibit striking axon-targeting specificity in spinal white matter, and this establishes the foundation for durable specificity of adult corticospinal circuitry. Based on this developmentally specified axon targeting specificity, we are able to define segmentally distinct CSN subpopulations through development into maturity: (1) CSN in lateral cortex that reside outside “classic” motor cortex and project only to bulbar-cervical targets (CSN_{BC-lat}); (2) CSN in medial sensorimotor cortex that project only to cervical segments and not beyond (CSN_{BC-med}); and (3) CSN that extend axons past thoracic T2 into caudal thoracic and lumbar spinal segments (CSN_{TL}) (Figure 1A). We also identified genes differentially expressed between bulbar-cervical (CSN_{BC}) and thoracolumbar (CSN_{TL}) projecting CSN subpopulations at critical developmental times. We identified that these segmentally distinct CSN subpopulations are molecularly distinct from the earliest stages of axon extension, and this molecular delineation goes beyond spatial separation in cortex.

In this study, we functionally investigate two top candidate controls that were identified using this differential transcriptomics approach: *Crim1* and *Kelch-like 14 (Klh14)*, genes for which there are no previously known functions in the central nervous system (CNS). In the accompanying study (Sahni et al., 2021), we identified that both these controls show remarkably specific expression by segmentally distinct CSN subpopulations during development; *Crim1* is a transmembrane protein expressed by CSN_{TL}, while *Klh14* belongs to the broad-complex, tramtrack, and bric a brac (BTB)-Kelch superfamily of proteins and is specifically expressed by CSN_{BC-lat}. Both genes also exhibit highly dynamic spatiotemporal expression: *Crim1* expression by CSN_{TL} peaks at P4, coincident with the peak of CSN_{TL} axon extension to distal spinal segments, while *Klh14* expression by CSN_{BC-lat} peaks early postnatally from E18.5 to P1, when these axons limit extension to proximal segments. We now employ gain- and loss-of-function approaches to identify that *Crim1* regulates thoracolumbar, while *Klh14* regulates bulbar-cervical, CSN axon targeting, respectively. These results provide tools for molecular investigation of the development of diverse yet specific functional output connectivity of cortex. Further, these results also provide the foundation for potentially investigating molecular bases of segmental targeting of other descending, spinal-projecting pathways.

RESULTS

CSN_{BC-lat} reside outside “classic” motor cortex (CSN_{BC-lat}) and project only to BC segments. CSN in medial sensorimotor cortex project either only to BC segments (CSN_{BC-med}) or past cervical to thoracolumbar segments (CSN_{TL}) (Sahni et al., 2021). These CSN subpopulations continue to exhibit distinct spinal axon projection and gray matter collateralization into maturity and are molecularly distinct well before final connectivity is established. *Crim1* is expressed by CSN_{TL}, while *Klh14* is expressed by CSN_{BC-lat} (Sahni et al., 2021; Figure 1B). This enables molecular delineation and prospective identification of these CSN subpopulations: (1) *Klh14* expression delineates *Klh14*-positive CSN_{BC-lat} from *Klh14*-negative CSN_{BC-med}; (2) all CSN_{TL} are *Klh14* negative; and (3) ~95% of CSN_{TL} express *Crim1* (Sahni et al., 2021; schematized in Figure 1A). This early axon extension specificity between CSN_{BC} and CSN_{TL} suggests early molecular specification; distinct subpopulations are molecularly controlled either to extend axons past thoracic T2 or to limit axon extension to cervical cord. We investigated whether these top candidate molecular controls—*Crim1* and *Klh14*—regulate differential axon targeting during development.

CSN are specified normally and project normally to the spinal cord in *Crim1*-null mice

We first investigated *Crim1* function in CSN_{TL} axon targeting. We generated *Crim1* nulls (Figures 1C–1C'') by outbreeding *Crim1*^{GCE} mice (Harding et al., 2011; STAR Methods) to a CD1 background to generate *Crim1*^{GCE} homozygotes, similar to Pennisi et al. (2007). *Crim1* nulls are smaller than wild-type (WT) or heterozygous littermates (Figures S1A and S1A') and survive to P28 with some perinatal lethality.

We first investigated overall CSN specification in *Crim1* nulls. Given predominantly postnatal expression of *Crim1*, projection neuron specification occurs normally in *Crim1*

nulls. Subcerebral projection neuron-specific controls *Fezf2* (Figures 1D–1D'') and CTIP2 (Figures S1B and S1B') are expressed normally, as are callosal projection neuron (CPN)-specific SATB2 (Figures S1C and S1C') and corticothalamic projection neuron (CThPN)-specific FOG2 (Figures S1D and S1D'). CSN_{medial}-specific and CSN_{BC-lat}-specific controls are also unaltered in *Crim1* nulls: CSN_{medial}-specific genes such as *Cry-mu* (Figures 1E–1E'') and *St6galnac5* (Figures S1E and S1E') are expressed normally, as are CSN_{BC-lat}-specific *Klhl14* (Figures S1F and S1F') and *Cartpt* (Figures S1G and S1G'). This indicates that CSN specification and differentiation (including CSN_{TL} in particular) occur normally without *Crim1* function. Consistent with normal overall molecular differentiation of CSN, retrograde labeling from cervical cord reveals that CSN axon extension to cervical C1 is unaffected without *Crim1* function (Figures 1F–1J).

Crim1 is required for CSN_{TL} axon extension toward thoracolumbar spinal segments

We next investigated developmental axon extension in *Crim1* nulls by what normally would have been CSN_{TL}. Retrograde labeling from lumbar/caudal thoracic cord (T13–L1) at P5 (when CSN axons first reach this level) revealed significantly fewer labeled lumbar-projecting CSN (CSN_L) in *Crim1* nulls (Figures 2A–2I' and 2J). We investigated whether other CSN might “compensate” for this deficit but found that there are no retrogradely labeled neurons outside the normal location of CSN_{TL} in medial cortex. Taken together, these results indicate that while CSN are normally specified and express other CSN_{medial} genes normally in *Crim1* nulls, they fail to extend axons to caudal thoracolumbar segments from the earliest developmental stages.

We next confirmed and extended these results via anterograde labeling. We injected AAV expressing EGFP into caudomedial cortex at P0 (Figure 2K) to visualize CSN_{TL} axons at P4. This enabled investigation of how far caudal CSN_{TL} axons project in the cord. We find that CSN_{TL} axons extend normally from cervical C1 to thoracic T2 in *Crim1* nulls (Figures 2L–2O). Quantification of labeled corticospinal tract (CST) fluorescence intensity finds no difference at T1–T2 (normalized to intensity at C1–C2; Figure 2R) in *Crim1* nulls compared to *Crim1* WT; *Crim1*-null CSN_{TL} axons appear to extend normally through the cervical cord to reach T2.

In striking contrast, *Crim1*-null CSN_{TL} axons exhibit significant reduction in extension from T2–L1 (Figures 2P and 2Q). We find a significant (~20%) reduction in CST intensity in *Crim1* nulls even by only 25% of the distance through the thoracic cord. This reduction persists until almost no axons reach the thoracolumbar junction (Figure 2S). In WT mice, ~20% (19% ± 4%) of axons that enter the thoracic cord extend to lumbar L1, and this axon population is almost completely absent in *Crim1* nulls (intensity at T13–L1 in *Crim1* nulls: 2% ± 1%). Therefore, these early lumbar projections are almost completely eliminated in *Crim1* nulls, suggesting that *Crim1* functions critically in what are likely the pioneer lumbar-projecting axons to enable their extension through thoracic and into lumbar cord. These data indicate that *Crim1* is specifically required by CSN_{TL} to extend axons through thoracic into lumbar spinal segments.

Reduction of axon extension to thoracolumbar segments in *Crim1*-null mice persists into maturity

We next investigated whether reduction in CSN axon extension to thoracolumbar segments at these early developmental times is maintained. We performed retrograde labeling from T13-L1 at P23 and analyzed the mice at P28. We find that early reduction in CSN axons reaching T13-L1 persists in P28 mice (Figure 2J).

Next, to rigorously investigate whether CSN remain in medial cortex, or whether they might have been eliminated potentially due to lack of targeting, we investigated expression of cardinal CSN-specific genes at P28 in *Crim1* nulls. We find that normal molecular development of CSN is maintained; subcerebral-specific *Fezf2* (Figures S2A–S2B') and CSN_{medial}-specific *Cry-mu* (Figures S2C–S2D') are expressed normally in P28 *Crim1*-null cortex. Therefore, even though CSN persist in more mature cortex in the position normally held by CSN_{TL}, they fail to extend axons to caudal thoracolumbar segments, even at maturity. This indicates that *Crim1* enables CSN_{TL} axon extension from early development at P4 into maturity at P28.

Crim1 functions cell autonomously in CSN_{TL} to enable axon extension to thoracolumbar spinal segments

Crim1 is expressed by developing spinal motor neurons (Kolle et al., 2000) and, we find, also by other spinal neurons (Sahni et al., 2021). CSN_{TL} axon extension deficits in *Crim1* nulls might therefore arise from CSN-intrinsic and/or CSN-extrinsic *Crim1* function. Arguing for centrally CSN-intrinsic function, the reduction in CSN_{TL} axon extension at P4 occurs prior to CSN axons encountering spinal neurons, while they are still traversing the dorsal funiculus. This suggests that axon extension deficits in *Crim1* nulls are not centrally due to spinal *Crim1* expression. We directly investigated the possibility of additional, likely smaller, non-CSN-intrinsic effects of spinally derived *Crim1* by evaluating potential rescue by cortical/CSN *Crim1* overexpression in *Crim1* nulls.

We used AAV-mediated gene delivery to express either EGFP alone (control) or EGFP plus *Crim1* (potential rescue). As controls, we injected AAV particles engineered to express EGFP into medial cortex at P0 in both WT ("WT" in Figure 3A) and *Crim1* nulls ("KO" [knockout] in Figure 3A'). In other *Crim1* nulls, we co-injected AAV particles engineered to express *Crim1* along with AAV EGFP ("KO + *Crim1*" in Figure 3A''). In separate experiments, we confirmed that this enables cortical *Crim1* overexpression (AAV-*Crim1*; Figures 4J and 4K). All mice were perfused at P7, and we investigated CSN_{TL} axon extension in the dorsal funiculus at C1-C2, T1-T2, and L1-L2 in WT (Figures 3B–3D), KO (Figures 3E–3G), and KO + *Crim1* (Figures 3H–3J) mice. Quantification at T1-T2 reveals no difference among all three groups, indicating normal CSN axon extension to T1-T2 in *Crim1* nulls (Figures 3C, 3F, and 3I). This confirms, at P7, our earlier findings at P4 (Figure 2R) that *Crim1* is not required for CSN_{TL} axon extension to T2.

We next investigated whether cortical-derived *Crim1* can rescue CSN axon extension to distal segments in the thoracolumbar cord (T13-L1) in *Crim1* nulls. At lumbar L1, there is clear qualitative reduction in the number of CSN axons present in *Crim1* nulls compared to

WT (Figures 3D and 3G). This confirms the findings at P4 (Figures 2P, 2Q, and 2S) that *Crim1* is necessary for CSN_{TL} axons to extend through thoracic cord to lumbar segments. Strikingly and importantly, this reduction is not observed in KO + *Crim1* mice (Figure 3J). Quantification of CST fluorescence intensity at L1-L2 reinforces these qualitative results. We find significant reduction in CSN axon extension to L1-L2 in *Crim1* nulls that received AAV-GFP alone (KO) compared to WT mice (CST intensity at L1-L2 normalized to C1-C2 in WT = 28% ± 2%, KO = 13% ± 2%; Figure 3K). In contrast, CST intensity at L1-L2 in KO + *Crim1* mice is statistically indistinguishable from WT mice (CST intensity at L1-L2 in KO + *Crim1* = 21% ± 7%; Figure 3K). This indicates that *Crim1* can CSN-autonomously rescue axon extension deficits to caudal thoracolumbar segments in *Crim1* nulls. The rescue might be even closer to WT than reported here, because while one of four mice in the KO + *Crim1* group appears to be an obvious outlier, the distribution of normalized CST intensity at L1-L2 in the other three KO + *Crim1* mice lies entirely within the WT range (Figure 3K). In the single outlier, the lumbar CST intensity is dramatically lower than any other mouse in any experimental or control *Crim1*-null subgroup. Though we include this outlier in the results above, it dramatically lowers the overall average CST intensity at L1-L2 in KO + *Crim1* mice (if this one outlier were excluded, the average CST intensity at L1-L2 in KO + *Crim1* mice would be 28% ± 3%, almost identical to average WT intensity, 28% ± 2%). Together, the timing of effect on CSN_{TL} axon extension combined with the rescue experiments reinforce that *Crim1* functions centrally intrinsically within CSN to enable CSN_{TL} axon extension to thoracolumbar segments.

***Crim1* misexpression in CSN_{BC-lat} redirects their axons to caudal spinal segments**

We next investigated whether *Crim1* can redirect CSN_{BC-lat} axons to thoracolumbar segments. We misexpressed *Crim1* in developing CSN_{BC-lat} at two distinct times and investigated their axon extension. We first introduced a *Crim1* expression construct into developing CSN_{BC-lat} via *in utero* electroporation at E12.5. While *Crim1* misexpression does not increase the number of CSN_{BC-lat} axons simply entering thoracic cord at T1-T2, *Crim1* misexpression in CSN_{BC-lat} does redirect the majority of these axons past their normal rostral targets to distal thoracic segments (Figures 4A–4C).

Crim1-overexpressing CSN_{BC-lat} (Figures 4D and 4E) do not activate endogenous *Crim1* expression (Figures 4F and 4G; *in situ* probes for detecting endogenous versus overexpressed *Crim1* are in Table S1). Further, *in utero* *Crim1* overexpression does not alter *Klhl14* expression (Figures 4H and 4I), suggesting that CSN_{BC-lat} differentiation is not affected by *Crim1* overexpression. However, there still remained the unlikely possibility that the effect on CSN_{BC-lat} axon extension is due to alterations in early CSN_{BC-lat} specification other than *Klhl14*, since overexpression by *in utero* electroporation begins in progenitors and continues into postmitotic neurons. We therefore next performed *Crim1* overexpression in CSN_{BC-lat} at P0 to directly investigate whether CSN_{BC-lat} axons can be redirected post-mitotically to thoracolumbar segments once their axons have reached the cord. We used AAV-mediated gene delivery to misexpress *Crim1* in CSN_{BC-lat}. We injected AAV-*Crim1* plus AAV-EGFP into rostralateral cortex at P0 (Figures 4J and 4K). *Crim1* overexpression by CSN_{BC-lat} is sufficient to direct many of their axons to thoracolumbar segments. While few axons from control (AAV-EGFP alone) CSN_{BC-lat} enter the thoracic cord, and no axons

extend even 25% through the thoracic cord (Figures 4L, 4N, and 4U; $n = 3$ mice), axons of AAV-Crim1-overexpressing CSN_{BC-lat} enter (Figures 4M, 4M', and 4O) and often traverse from 50% to the entire length of the thoracic cord (Figures 4M and 4O; $n = 3/3$ *Crim1*-overexpressing mice display CSN_{BC-lat} axons halfway through thoracic, Figure 4M''; and two of them display axons through the entire length of the thoracic cord, Figure 4M'''). Together, these experiments—Crim1 loss-of-function, rescue of CSN_{TL} axon extension by *Crim1* overexpression in Crim1-null cortex, and Crim1 misexpression redirecting CSN_{BC-lat} axons—indicate that Crim1 centrally, and predominantly cell intrinsically, controls CSN axon extension to caudal thoracolumbar segments. These data also reveal that Crim1 does not mediate CSN axon extension to thoracic T2. Rather, Crim1 regulates CSN axon extension past T2 into thoracolumbar cord.

Reduction in *Klhl14* function causes aberrant CSN_{BC-lat} axon targeting beyond the cervical cord

We investigated *Klhl14* function in CSN_{BC-lat} axon targeting as schematized in Figure 5A. We first introduced a short hairpin RNA (shRNA) construct that effects ~85% knockdown of *Klhl14* expression into lateral cortex using *in utero* electroporation to disrupt *Klhl14* expression in developing CSN_{BC-lat} (Figures 5A, S3A, and S3B). We first confirmed that EGFP+ neurons in both control and *Klhl14*-shRNA-electroporated mice were located laterally throughout the rostro-caudal extent of sensorimotor cortex (Figures S3D and S3E); quantification established no fluorescence in medial cortex in either group (Figure S3F; i.e., electroporations specifically targeted CSN_{BC-lat}, enabling investigation of CSN_{BC-lat} axon targeting). *Klhl14* shRNA does not appear to disrupt neuronal differentiation or lamination (e.g., *Klhl14*-shRNA-expressing CSN_{BC-lat} express normal levels of CTIP2; Figure S3C). CSN_{BC-lat} axon collateralization in the P4 cervical cord (C2-T1) is similarly unaltered between control and *Klhl14* shRNA-electroporated mice (data not shown).

We next investigated whether *Klhl14* functions to normally restrict CSN_{BC-lat} axon targeting in the dorsal funiculus. At P4, while almost all axons from control, scrambled shRNA-expressing CSN_{BC-lat} extend only within cervical cord (only $6\% \pm 3\%$ of CSN_{BC-lat} axons at cervical C1 extend to thoracic T1-T2; Figure 5J), significantly more axons from *Klhl14*-shRNA-expressing CSN_{BC-lat} extend to T1-T2 ($21\% \pm 5\%$; Figures 5B–5E and 5J). The rare control axons that enter the thoracic cord are limited to the first few thoracic segments (assessed from T2-L1). Further, these rare control CSN_{BC-lat} axons never extend collaterals in the thoracic cord (Figure 5F).

In striking contrast, many axons from *Klhl14*-shRNA-expressing CSN_{BC-lat} extend significantly further, reaching as far as 75% of the distance through thoracic cord (Figures 5G–5I' and 5K), and they extend branching collaterals even at mid-thoracic levels (Figures 5H' and 5I').

These aberrantly extended CSN_{BC-lat} axons remain in thoracic cord even at P14 (Figures S4K–S4N'). Because this is past the period of normal *Klhl14* expression in CSN_{BC-lat}, this indicates that early *Klhl14* control over CSN_{BC-lat} axon extension is critical in establishing CSN_{BC-lat}-specific connectivity in the mature CNS. Consistent with CSN specificity (in particular, CSN_{BC-lat}) of *Klhl14* expression, there are no axon targeting defects by CPN

(Figures S4E–S4H) in *Klh14*-shRNA-electroporated cortex. Taken together, these results identify that *Klh14* specifically limits CSN_{BC-lat} axon extension and branching proximal to T2.

***Klh14* functions in postmitotic CSN_{BC-lat} specifically when CSN axons are extending into the spinal cord**

Because CSN_{BC-lat} and CSN_{medial} do not exhibit different rates of axon extension (Sahni et al., 2021), it is not likely that *Klh14* limits CSN_{BC-lat} axon extension to the cervical cord by inhibiting the rate of axon extension. We directly investigated this unlikely, but still theoretical, possibility. We examined control-versus *Klh14*-shRNA-expressing CSN_{BC-lat} axons at earlier developmental times in case a reduction of *Klh14* function causes CSN_{BC-lat} axons to grow faster into thoracic cord, thus past their normal targets. At P0, when CSN axons first reach the cord, there is no difference in length of axon growth between control-shRNA- and *Klh14*-shRNA-expressing CSN_{BC-lat} (Figures S4A–S4D). These data indicate that *Klh14* does not regulate rate of axon extension. Rather, these data indicate that *Klh14* regulates the specificity of CSN_{BC-lat} axon targeting (i.e., to restrict CSN_{BC-lat} axons from extending beyond T2).

These results also suggest that *Klh14* functions while CSN_{BC-lat} axons are extending in the cord, consistent with the time course of *Klh14* expression in CSN_{BC-lat} : *Klh14* expression peaks early at E18.5 and P1, then gradually declines from P4 to P10, and expression is completely absent by P14 (Sahni et al., 2021). However, there remained the unlikely possibility that *Klh14* shRNA alters CSN_{BC-lat} differentiation before their axons reach the cord, ultimately causing aberrant axon extension later at P4. To directly investigate this unlikely possibility, and to delineate the specific temporal requirement of *Klh14* function, we generated conditional *Klh14* mice in which the second coding exon of *Klh14* is flanked by loxP sites.

To conditionally ablate *Klh14* function postmitotically, we co-injected AAV-Cre and AAV-FLEX-tdTomato at P0 into lateral cortex of *Klh14*^{flox/flox} (*Klh14* conditional KO [cKO]) and *Klh14* WT as controls (Figure 6A). This manipulation leaves *Klh14* function intact through birth and early postmitotic differentiation of CSN_{BC-lat} ; *Klh14* function is ablated only as CSN_{BC-lat} axons are reaching the cord. We investigated CSN_{BC-lat} differentiation and axon extension at P7 using the AAV-FLEX-tdTomato reporter (tdTomato is expressed only by neurons also receiving AAV-Cre). We first confirmed deletion of *Klh14* expression in lateral cortex in AAV-Cre-injected hemisphere in *Klh14* cKO mice (Figures S5A and S5B). Fully consistent with results using *Klh14* shRNA, this postmitotic conditional deletion of *Klh14* does not alter CTIP2 expression and, thus, does not disrupt overall subcerebral projection neuron differentiation of CSN_{BC-lat} (Figure S5C).

We next investigated CSN_{BC-lat} axon extension in the cord. We first confirmed the consistency of AAV injections in lateral cortex in WT and *Klh14* cKO mice via whole-mount images (Figure 6B and 6C). We verified that there was no labeling in medial cortex in WT and *Klh14* cKO mice (Figures S5D–S5F). We next investigated CSN_{BC-lat} axon extension in WT and *Klh14* cKO mice by analyzing tdTomato+ axons in dorsal funiculus at cervical C1-C2 and thoracic T1-T2. At P7, consistent with our prior anterograde analyses,

>95% of all CSN_{BC-lat} axons in WT mice terminate in the cervical cord, with only rare axons present at T1-T2 (Figure 6D and 6E). In contrast, significantly more CSN_{BC-lat} axons project to T1-T2 in *Klhl14* cKO mice (Figures 7F and 7G). Quantification of CST fluorescence intensity at T1-T2 reveals a 2.8-fold increase in the number of CSN_{BC-lat} axons that extend to T1-T2 in *Klhl14* cKO versus WT mice (CST intensity at T1-T2 normalized to C1-C2: *Klhl14* WT = 3.2% ± 1.2%; *Klhl14* cKO = 9.3% ± 1.5%; Figure 6H). This indicates that significantly more CSN_{BC-lat} axons extend into thoracic cord upon postmitotic conditional deletion of *Klhl14*. These aberrantly extended CSN_{BC-lat} axons in *Klhl14* cKO mice also collateralize in the thoracic gray matter (Figure 6I–7L'), similar to *Klhl14*-hRNA-expressing CSN_{BC-lat}.

The shRNA and cKO results both indicate very similar increases in CSN_{BC-lat} axon extension to thoracolumbar segments using two independent approaches (~3.5-fold using shRNA, ~2.8-fold using the conditional null). Further, the results with Cre-dependent conditional gene deletion in *Klhl14* cKO mice delineate a temporal, postmitotic requirement of *Klhl14* function in regulating CSN_{BC-lat} axon extension, when these decisions are being executed in the spinal cord.

Reduction or deletion of *Klhl14* function causes ectopic *Crim1* expression in lateral cortex

We also investigated whether this aberrant CSN_{BC-lat} axon extension into thoracic cord with loss of *Klhl14* function might be accompanied by other CSN_{TL}-like changes (e.g., changes in *Crim1* expression). We find that *Crim1* is aberrantly expressed in lateral cortex at P4 in *Klhl14*-shRNA-electroporated mice (Figure 7A and 7B; compare 7B' with 7B''). However, not all CSN_{TL} genes are aberrantly expressed (e.g., CSN_{medial} genes *Cry-mu* and *Cdh8* remain restricted to medial layer V after *Klhl14*-shRNA electroporation; Figures S6A–S6D). *Klhl14* cKO mice display similar, aberrant *Crim1* expression in lateral cortex in the AAV-Cre-injected hemisphere (Figure 7C and 7D; compare 7D' with 7D''). These results by two independent experimental approaches to *Klhl14* loss-of-function indicate that the population of CSN_{BC-lat} becomes more CSN_{TL}-like upon loss of *Klhl14* function, in both its aberrant axon extension and gene expression.

Finally, to investigate whether *Klhl14* might be sufficient to restrict axon targeting to cervical cord, we misexpressed *Klhl14* in medial cortex. We injected AAV-*Klhl14* into medial cortex and examined CSN_{TL} axon extension to thoracolumbar targets. We find no effect on CSN_{TL} axon extension as assessed by both anterograde (Figures S7C–S7E) and retrograde (Figures S7A and S7B) analyses. These data additionally indicate that *Klhl14* does not control CSN_{BC-lat} axon elongation by simply regulating rate of axon extension. Together, these results indicate that *Klhl14* is necessary but not sufficient to limit CSN_{BC-lat} axons to cervical cord.

DISCUSSION

Segmentally precise CSN connectivity enables highly skilled motor control (and related “top-down” sensorimotor feedback and autonomic functions). Further, CSN are clinically relevant; individual human neurodegenerative diseases predominantly affect segmentally specific CSN (e.g., bulbar amyotrophic lateral sclerosis [ALS] or hereditary spastic

paraplegias [HSPs]). The molecular bases for development of such segmental specificity by CSN are not known.

In this report and the accompanying paper (Sahni et al., 2021), we identify that distinct CSN subpopulations are molecularly specified during development to target distinct spinal segments at maturity. We identify molecular controls that distinguish during development anatomically, hodologically, and likely later functionally distinct CSN subpopulations, and they govern differential axon targeting of CSN at T2. These controls establish the first stages of a dual-directional set of complementary controls over critical motor circuitry.

Mechanisms controlling differential axon extension by CSN subpopulations

Crim1 and Khlh14 have no previously reported function in the CNS. Gain- and loss-of-function results indicate that Crim1 does not mediate CSN axon extension to T2 but affects axon extension past T2 into thoracic cord. Axon extension abnormalities are apparent by ~25% of the rostro-caudal distance through thoracic cord and are maintained more distally, with a small subset of CSN_{TL} axons extending to lumbar cord (Figure 2). Crim1 might function in “pioneer” lumbar-projecting CSN axons to enable extension through thoracic into lumbar cord. However, Crim1 appears to not function alone; retrograde labeling at P28 identified only ~50% reduction in CSN projections to lumbar cord in Crim1 nulls (Figure 2J), indicating that some CSN_{TL} axons extend to distal targets independent of Crim1. Interestingly, spared lumbar-projecting CSN without Crim1 function reside in the typical medial location, indicating that there is no anatomically distinct, alternate Crim1-independent lumbar-projecting CSN subpopulation. Crim1 rescue in Crim1 nulls indicate that Crim1 functions autonomously in CSN.

Crim1 is a transmembrane protein with a large extracellular domain containing cysteine-rich repeats (CRRs) that can bind multiple growth factors (e.g., bone morphogenetic proteins [BMPs] and transforming growth factor β [TGF- β]). BMPs can function in axon guidance (Charron and Tessier-Lavigne, 2005; Salie et al., 2005). The Crim1 ortholog in *Drosophila* motor neurons controls growth of neuromuscular junctions, regulating BMP levels (James and Broihier, 2011). Crim1 might enable or direct CSN_{TL} axon extension to distal segments by acting as a guidance receptor. Crim1 has a predicted IGF-binding motif (Kolle et al., 2000) that might augment IGF-I signaling to drive CSN_{TL} axon extension (Ozdinler and Macklis, 2006). *Crim1* levels in CSN_{TL} peak during axon extension to distal targets (Sahni et al., 2021) and are sufficient to direct thoracolumbar axon extension by CSN_{BC-lat} (Figure 4). Both expression and temporal control of Crim1 levels might serve to direct long CSN_{TL} axon extension. Alternatively, Crim1 might cause CSN_{TL} axons to not recognize the cervical cord as an appropriate target region and, thus, to extend to distal targets, potentially by recognition of cues in the extracellular matrix. Crim1 is known to regulate β 1 integrin-mediated cell adhesion in the developing lens (Zhang et al., 2016); a similar mechanism might regulate CSN_{TL} axons.

We identify that Khlh14 limits CSN_{BC-lat} axons to cervical cord. Khlh14 might function in multiple distinct ways: by instructing CSN_{BC-lat} axons to not cross T2; by instructing CSN_{BC-lat} axons to recognize brainstem and cervical cord as appropriate targets; or a combination of these mechanisms. Though Kelch family members are reported to regulate

cytoskeletal dynamics, this does not appear to be a mechanism of *Klhl14* limiting CSN_{BC-lat} axon extension.

Crim1 expression during early development largely predicts thoracolumbar projection at maturity (CSN_{TL}) (Sahni et al., 2021). *Crim1* might be transcriptionally repressed in CSN_{BC}. Consistent with this, *Crim1* overexpression redirects a subset of CSN_{BC-lat} axons to caudal thoracic cord. Loss of *Klhl14* function by two distinct approaches results in aberrant CSN_{BC-lat} axon extension into thoracic cord; this is accompanied by ectopic *Crim1* expression in lateral cortex. This suggests that *Crim1* regulation might be critical to limit CSN_{BC-lat} axons to cervical cord.

In both *Klhl14* loss-of-function and *Crim1* gain-of-function experiments, even those CSN_{BC-lat} axons that aberrantly extend into thoracic cord do not exit into lumbar cord. In contrast, cortical/CSN *Crim1* overexpression in *Crim1* nulls is sufficient to direct CSN_{TL} axons to caudal thoracic segments and even to extend past thoracic segments into lumbar cord. Together, these results suggest that a subset of CSN_{TL} possesses additional mechanisms enabling them to project past thoracic into lumbar segments, if *Crim1* is present to enable them to traverse the thoracic cord. This is consistent with our earlier results that lumbar-projecting CSN (CSN_L) are a distinct subset within CSN_{TL}, both spatially (most caudal among CSN_{TL}) and, seemingly, molecularly (a subset of CSN_{TL} genes expressed only in the caudal CSN_{TL} domain) (Sahni et al., 2021). CSN_L might rely on a subset of CSN_{TL} molecular controls that are CSN_L specific to direct or enable CSN_L axons to enter the lumbar cord.

Finally, these results highlight that understanding development of segmental specificity of corticospinal circuitry benefits substantially from investigation at early developmental times, well before CSN axon collaterals invade the spinal gray matter or synaptic connectivity is even established. This is further highlighted by the fact that some molecular regulators (e.g., *Klhl14*) are no longer expressed past the first postnatal week, after this initial development is complete. Therefore, previous or future work not focused on these early developmental stages would be predicted to not identify at least some important early regulators of CSN axon targeting. This is especially relevant to recent work investigating neuronal diversity, particularly in adult motor cortex via single-cell transcriptomics (Yao et al., 2020), since these approaches after early development has ended would be predicted to not identify such transiently expressed early regulators, even if sequencing depth were sufficient.

Differential CSN axon targeting at thoracic T2 might reflect differential CSN-extrinsic cues

The divergent axon guidance decisions by CSN subpopulations at T2 likely reflect distinct, differential responses of their growth cones to distinct environmental cues (Raper and Mason, 2010) presented at the transition between these spinal segments. The specification of columnar identity along the rostral-caudal axis in the spinal cord is mediated by Hox expression patterns in spinal motor neurons, directing differentiation of distinct motor neuron pools at distinct spinal levels, particularly limb innervating at cervical versus autonomic neurons at thoracic levels (Dasen et al., 2003). Guidance cues, potentially downstream of Hox genes, might be differentially expressed between cervical and thoracic segments. CSN axon guidance decisions occur prior to collateral extension into gray matter.

Therefore, it appears likely that such cues might be presented by spinal white matter glia (e.g., molecularly distinct astrocytes along the dorsoventral axis in the cord encode positional cues to direct development of specific spinal neurons; Molofsky et al., 2014).

Implications for CSN function, plasticity, evolution, and disease vulnerability

Although the CST in rodents has been mostly thought to control forelimb movement, it also controls elements of hindlimb control (Serradj et al., 2014). Motor analysis of *Crim1* nulls could be used to address some of these questions. Future investigations using *Crim1* cKO mice (Chiu et al., 2012) could be employed to investigate functional consequences of a lack of CSN_{TL} innervation in distal spinal segments.

It is intriguing to speculate whether molecular controls over segmentally specific connectivity during development might be altered and/or re-activated in instances of corticospinal plasticity in the adult CNS following disease or injury. For instance, CSN residing in hindlimb motor cortex sprout new collaterals in the cervical cord after a thoracic spinal cord injury (Ghosh et al., 2010) or after an ischemic stroke in forelimb motor cortex (Starkey et al., 2012). The results presented here might also shed light on such plasticity. While CSN_{TL} fail to extend axons to their distal spinal targets in *Crim1* nulls, they still persist into maturity. It is intriguing to speculate that these CSN_{TL} might display aberrant connectivity in the cervical cord, potentially mimicking the effects noted after adult CST injury described above. Future investigations into spinal connectivity of misrouted CSN axons after *Crim1/Klhl14* loss-of-function could begin to address such questions.

Loss of *Klhl14* function results in ectopic *Crim1* expression by CSN_{BC-lat} (Figure 7), indicating what appears to be a hierarchical order of controls over CSN segmental targeting. These results raise the intriguing possibility that CSN_{BC}-specific controls such as *Klhl14* evolved to suppress potentially older, “default” controls such as *Crim1*, enabling increased numbers and diversity of CSN projecting to the most dexterous control circuits in the cervical cord and functionally distinguishing CSN_{BC} from evolutionarily older CSN_{TL} subpopulations. This might underlie the extraordinary evolutionary expansion of skilled forelimb movements, since even subtle changes in nervous system organization can cause large behavioral changes (Katz and Harris-Warrick, 1999).

CSN degeneration in ALS, along with degeneration of spinal motor neurons, causes spasticity and paralysis (Bruijn et al., 2004). ALS and related motor neuron disorders involving CSN do not affect all CSN equally; in bulbar forms of ALS, brainstem-projecting CSN degenerate preferentially, while in HSP, primarily lumbar-projecting CSN degenerate (Salinas et al., 2008). It appears increasingly likely that such selective vulnerability might arise, at least in part, from dysregulation of developmental control over differential axon targeting by CSN subpopulations. Consistent with this, human *Crim1* maps close to a spastic paraplegia locus (Kolle et al., 2000), suggesting one such potential link to subtype-specific CSN disease. The *Crim1* function identified here adds credence to the hypothesis that dysregulation of early development might underlie selective CSN vulnerability in some motor neuron disease.

The work presented in this paper is a first step toward understanding how segmentally specific corticospinal organization is initially established during development; this segmentally specific circuitry would eventually include motor, sensory, and autonomic circuit organization and control. Even if regulators of early axon targeting (e.g., *Crim1*, *Klhl14*) do not establish functionally specific (e.g., motor versus autonomic) circuits, there are likely such regulators that work combinatorially with these early controls. Therefore, axon targeting specificity likely establishes the first stage of ultimate connectivity and functional specialization.

Delineation of gene sets highly specifically expressed by CSN_{BC} versus CSN_{TL} reveals a molecular network controlling connectivity rostral and caudal to T2. *Crim1* and *Klhl14*, on their own, are insufficient to fully explain this specificity. We present these as exemplar regulators of what are likely to be downstream growth-cone-located subcellular mechanisms of segmentally distinct axon targeting. Future investigations building from this work will likely identify increasingly detailed mechanisms (both CSN-intrinsic and CSN-extrinsic cues in the cord) that effect precision of axon targeting. Other identified subpopulation-specific genes have promise to elucidate additional intersectional levels of precision, potentially including additional segmental delineation, axon branching and connectivity within segments, and potentially even mono-versus bi-synaptic corticospinal-spinal connectivity. In this regard, we have functionally investigated additional candidates. These include the extracellular matrix protein Lumican as controlling spinal-segment-specific axon collateralization, rather than controlling axon targeting in spinal white matter (Itoh et al., 2021). Future investigation of interactions and hierarchical organization of these molecular regulators offers potential elucidation of development, organization, disease, and regeneration of corticospinal connectivity.

STAR★METHODS

RESOURCE AVAILABILITY

Lead contact—Further information and requests for resources and reagents should be directed to and will be fulfilled by the lead contact, Dr. Jeffrey D. Macklis (jeffrey_macklis@harvard.edu).

Materials availability—We plan to deposit *Klhl14^{flox}* mice to the Jackson Laboratory or MMRC. All unique/stable reagents generated in this study are available with a materials transfer agreement from the lead contact for academic, non-commercial use; negotiation and completion of a materials transfer agreement with Harvard University is required if there is potential for commercial application.

Data and code availability—Microscopy data reported in this paper will be shared by the lead contact upon request.

No original code was generated as part of this study.

Any additional information required to reanalyze the data reported in this paper is available from the lead contact upon request.

EXPERIMENTAL MODEL AND SUBJECT DETAILS

Mice used in this study—Wild-type mice on a pure C57BL/6 background were obtained from Charles River Laboratories (Wilmington, MA). The day of vaginal plug detection was designated as E0.5. The day of birth was designated as P0. All mouse studies were approved by the Harvard University IACUC, and were performed in accordance with institutional and federal guidelines.

Crim1^{GCE} mice (Harding et al., 2011) were obtained from Jackson Laboratories (stock number 017495); they contain an EGFP coding sequence followed by a tamoxifen-inducible Cre recombinase coding sequence placed 3' to the ATG of the first codon. The original depositing investigator observed no EGFP expression, and we confirm no EGFP expression at any age.

To obtain Crim1^{GCE} homozygous null mice, we backcrossed males from the original line (maintained on a C57BL/6 background) with WT CD1 females. At each generation, transgenic males were mated with WT CD1 females. Mixed background (F6) transgenic heterozygote mice were mated to generate Crim1 nulls. To distinguish Crim1^{GCE} WT, heterozygous and homozygous null mice, the following primers were used:

WT allele—Forward – 5' - GCAGGAGGATGTACTTGGTG - 3'

Reverse – 5' – TGTGTCTATGCGTGTCGG - 3'

GCE allele—Forward – 5' - AAGTTCATCTGCACCACCG - 3'

Reverse – 5' – GTTATTCGGATCATCAGCTACACC - 3'

Klh14 conditional allele mice were generated using embryonic stem cells obtained from the KOMP Repository (<https://www.komp.org>). The mouse strain was created from embryonic stem cells clone EPD0735_1_H02, obtained from the KOMP Repository and generated by the Wellcome Trust Sanger Institute (WTSI). Targeting vectors used were generated by the WTSI and the Children's Hospital Oakland Research Institute as part of the Knockout Mouse Project (3U01HG004080). Methods used on the organization and generation of CSD targeted alleles have been published (Skarnes et al., 2011). Targeted embryonic stem cells clones were injected into blastocysts at the Harvard Genome Modification Facility, and the chimeras were bred with C57BL/6J albino mice (Jackson Laboratories; stock number 00058). Positive pups with black coat color were first confirmed using genotyping PCR. Per KOMP recommendation, correct gene targeting was then confirmed in the founder and in subsequent litters from these founders using long range PCR. The initial (Klh14-lacZ knock-in knock out) mice were then bred with R26-FlpO mice (Jackson Laboratories; stock number 12390) to obtain Klh14 floxed mice as described (Skarnes et al., 2011), which were then bred to homozygosity. To distinguish between the Klh14 WT versus Klh14^{fllox} allele, the following genotyping primers were used:

Klh14 Forward—TTCTTAGTGCCCTTTCCTCCGTACC

Klh14 Reverse—ATGAAACTCTGGTGGCTTTGGATGC

The genders of early postnatal mice were not determined. Mice were used at the following ages:

Crim1^{GCE} mice: were used at P4, P7, P28, and as adults.

Klhl14^{flox} mice: were used at P7, and as adults.

METHOD DETAILS

Anterograde and retrograde labeling—Retrograde labeling was performed as described in the accompanying study (Sahni et al., 2021). Briefly, we used a pulled glass micropipet attached to a nanojector (Nanoject II, Drummond Scientific, Broomall, PA) to bilaterally inject the retrograde label Cholera Toxin B subunit (CTB; Thermo Scientific) into specific spinal levels on each side of the midline using ultrasound backscatter microscopy (Vevo 770; VisualSonics, Toronto, Canada). For cervical labeling (P3), we used the fourth ventricle in the medulla, and the spinal-medullary junction as landmarks. The landmark for labeling CSN whose axons reach thoracic T12/13 -lumbar L1 was established by examining the relative position of the vertebral column as it approaches the dorsal surface of the body (moving from caudal thoracic levels rostrally, where the column is located more deeply and closer to the viscera, to lumbar levels caudally, where the column is situated closer to the dorsal surface). The central landmarks for all intraspinal injections are as described (Sahni et al., 2021)—the midline, vertebral bodies, dorsal aspect of the spinal cord, and echo density in the dorsal funiculus. For these neonatal injections, pups were anesthetized under ice for 4 minutes. The pups were placed on a heating pad for recovery.

To retrogradely label CSN projecting to T/13-L1 in adults, we anesthetized mice using isoflurane anesthesia (2.5% isoflurane in 100% oxygen). We exposed the caudal thoracic and rostral lumbar vertebrae under standard aseptic surgical procedures (n = 3 each for Crim1^{GCE} WT and homozygous null mice). Using L1 as a landmark, we used bone rongeurs (World Precision Instruments) to create a small window in the L1 dorsal vertebral lamina to expose the dura. A rolled gauze was placed under the mouse's abdomen to slightly elevate the lumbar cord. The spine was gently stretched, and the tail was taped to maintain a flat spine for injection. Throughout each injection, the dura and cord were kept moist using warm, sterile saline. We injected 300 nL CTB-555 on either side of the midline using the same injection technique as for postnatal injections. After each injection, micropipettes were left in the spinal cord for an additional 1 min before withdrawal. Following each injection, wounds were closed using wound clips (AUTO-CLIP®, Becton Dickinson). Post-surgical care was performed as previously described (Greig et al., 2016). Mice were perfused 5 days later.

For AAV-mediated anterograde labeling, AAV2/1 particles expressing fluorescent protein were injected at P0 into specific cortical sub-regions under guidance by ultrasound backscatter microscopy, as described (Sahni et al., 2021). The central landmarks for the intracranial injections that provide both accuracy and precision are the midline, dorsal and lateral aspects of the lateral ventricle, anterior aspect of the hippocampus, posterolateral aspect of the striatum, corpus callosum, and its genu. All virus work was approved by

the Harvard Committee on Microbiological Safety, and conducted according to institutional guidelines.

Klh14 shRNA constructs—We obtained shRNAmir sequences, which are based on a microRNA-based RNAi (cloned in the pGIPZ lentiviral vector) specifically developed to highly effectively knock down Klh14 expression (Open Biosystems). In these plasmids, a CMV promoter drives the shRNA and an EGFP reporter. We tested the efficacy of each shRNA *in vitro* using the psi-CHECK2 luciferase system (Promega, Madison, WI) in 293T HEK cells using the manufacturer's instructions. The Klh14 coding sequence was cloned into the psi-CHECK2 vector (Promega, Madison, WI) downstream of the STOP codon in the renilla luciferase gene. Luciferase activity was measured using the Dual-Luciferase Reporter 1000 Assay System (Promega) on a Victor3 1420 plate reader (Perkin Elmer, Waltham, Massachusetts). Efficacy was assessed by comparing luciferase activity of each hairpin with a scrambled shRNA control. The following hairpin sequence gave the strongest knock down (> 85%):

5'-TGCTGTTGACAGTGAGCGACCTGTGTACCCTACAACAAATTAGTGAAGCCA

CAGATGTAATTTGTTGTAGGGTACACAGGCTGCCTACTGCCTCGGA-3' (mature hairpin sequence: 5'-CTGTGTACCCTACAA-CAA—3'). This sequence targets the 3' end of the Klh14 cDNA just prior to the STOP codon. We subcloned this hairpin into a separate plasmid, where it was placed 3' to an EGFP coding sequence, driven by a strong chicken beta actin (CBA) promoter (since the CMV promoter is known to be silenced in neural progenitors), and re-confirmed the efficacy in this new backbone. This CBA-driven plasmid was used in the *in vivo* experiments.

In utero electroporation—Surgeries were performed as previously described (Greig et al., 2016; Molyneaux et al., 2005). For Klh14 shRNA experiments, the following plasmids were used: pCBA-EGFP-Klh14 shRNA; pCBA-EGFP-scrambled shRNA (schematized in Figure 5A). For Crim1 overexpression, *Crim1* cDNA was placed 3' to the EGFP coding sequence, driven by the CBA promoter, with the two ORFs separated by a t2A linker sequence. In the control plasmid, Crim1 cDNA was replaced with a STOP codon 3' to the t2A linker sequence. 2 µg of either plasmid was diluted in PBS for electroporation.

Generation of AAV particles—Adeno associated viral (AAV) 2/1 particles were generated as described (Sahni et al., 2021). Viral particles were generated at the Massachusetts General Hospital Virus Core using established protocols (Maguire et al., 2013). Enhanced green fluorescent protein (EGFP) (for AAV-EGFP), and Crim1 (for AAV-Crim1) coding sequences were cloned into a shuttle plasmid (obtained from the core) that contains the following elements flanked by AAV2 ITRs: a CMV/ β -actin promoter to drive the expression of the gene of interest, followed by the woodchuck hepatitis virus post-transcriptional regulatory element (WPRE), a bovine GH pA signal, and an SV40 pA signal. For Crim1 overexpression, AAV-Crim1 particles were co-injected with AAV-EGFP particles (independent experiments with AAV-EGFP and AAV-tdTomato particles confirmed > 95% co-infection efficiency upon co-injection (data not shown)).

For *Klhl14* overexpression, *Klhl14* cDNA was placed 3' to the EGFP coding sequence; the two ORFs were separated by a t2A linker sequence. In this plasmid, WPRE was removed in order to include the entire construct under 4.1 kb (between the 2 ITRs). For both *Crim1* and *Klhl14* overexpression constructs, plasmids were transfected into HEK293T cells, and overexpression was confirmed *in vitro* using western blot analyses.

AAV8 hsyn-GFP-Cre was obtained from the vector core at the University of North Carolina at Chapel Hill (UNC Vector Core). AAV2/1 CAG-FLEX-tdTomato (originally generated by the Allen Institute) was obtained from the vector core at the University of Pennsylvania. Both viral particles were co-injected into lateral cortex as schematized in Figure 6A.

Immunocytochemistry and *in situ* hybridization—Brains were fixed and stained using standard methods (Galazo et al., 2016; Greig et al., 2016; Woodworth et al., 2016). Primary antibodies and dilutions used: rat anti-CTIP2, 1:500 (Abcam); rabbit anti-FOG2, 1:250 (Santa Cruz); chicken anti-GFP, 1:500 (Invitrogen); rabbit anti-GFP, 1:500 (Invitrogen); 1:500 rabbit anti-RFP (Rockland Immunochemicals), mouse anti-SATB2, 1:500 (Abcam). *In situ* hybridization was performed as previously described (Galazo et al., 2016; Greig et al., 2016; Woodworth et al., 2016). cDNA clones for riboprobes are listed in Table S1.

Imaging and quantification—Analysis of retrogradely labeled CSN comparing *Crim1* WT and null mice was performed as described in the accompanying study (Sahni et al., 2021). For analyzing CSN retrogradely labeled from cervical C1-C2, 50 μ m coronal brain sections of retrogradely labeled brains were imaged on an Axioscan Z1. For cell counts of retrogradely labeled CSN (from cervical cord) in *Crim1* null mice, we matched coronal sections of labeled cortices at 4 *a priori* designated levels (rostral to caudal as in Sahni et al. [2021]; images in Figure 1) in WT, het, and homozygous null mice. Cortices were binned into 5 medio-lateral bins spanning the width of each cortical hemisphere, and medial versus lateral distinction was made by combining the 3 medial bins for medial CSN counts and the 2 lateral bins for lateral CSN counts (as in Sahni et al., 2021). For counts of retrogradely labeled CSN_L (for retrograde label injection from caudal thoracic cord), we first dissected the spinal cord to confirm the matched spinal level of the retrograde label injection. Following confirmation, we analyzed coronal sections of each labeled cortex at three distinct rostro-caudal levels selected by *a priori* criteria (images shown in Figure 2). In all mice, regardless of genotype, labeled CSN_L were located only in medial cortex. Matched sections were imaged, and every labeled neuron was counted in each section, using the Cell Counter function in ImageJ.

For unbiased tracing of EGFP+ CSN_{BC-lat} axons in the dorsal funiculus (Figures 4N and 4O), we used the thresholding function in NIH ImageJ. Thresholding criteria were established *a priori* and then applied to the dorsal funiculus in each monochrome image of the horizontal section of the thoracic spinal cord.

For all CST quantification on axial sections, 60X confocal Z stacks of the entire CST in the dorsal funiculus were obtained on either a BioRad Radiance 2000 or Zeiss LSM 780

confocal microscope. Cervical, thoracic, and lumbar cord axial sections were imaged using identical parameters.

For axon extension experiments, the thoracic cord was sectioned either sagittally or horizontally. Every section that contained a labeled axon was imaged using an ANDOR Clara DR328G camera (ANDOR Technology, South Windsor, CT) mounted on a Nikon Eclipse 90i microscope (Nikon Instruments). Each section was imaged in its entirety, from rostral to caudal and in the Z axis. These Z stacks were collapsed using the “create focused image” function on the NIS-Elements acquisition software (Nikon Instruments), and converted to monochrome images.

For axon counts in Kihl14-shRNA experiments, we analyzed 3 axial sections each at cervical and thoracic levels and averaged the axon counts. For all fluorescence intensity quantification on axial sections we imaged 2 sections at each spinal level per mouse. We selected the dorsal funiculus as the region of interest (ROI) on all images in Adobe Photoshop. Fluorescence intensity of the labeled CST was then measured in each ROI in monochrome images using ImageJ, and the intensity was averaged at each spinal level. CST fluorescence was normalized to intensity measured at cervical C1, and expressed as a percentage at thoracic and lumbar levels.

For axon extension measurements on horizontal spinal cord sections, we selected 610×640 pixel sections of each image of each spinal cord section, at five *a priori* designated intervals (rostral-most, 25%, 50%, 75%, and caudal most). In each image, the CST was then additionally selected as an ROI in Adobe Photoshop. For all intensity measurements, images first had threshold adjustment using the Feature J function on ImageJ, such that intensity on unlabeled parts of the spinal white matter (without a labeled axon) was zero. Intensity of the ROI was then quantified using the Analyze Particles function on ImageJ. Intensity at each rostro-caudal level was integrated across multiple sections, then normalized to the intensity at the rostral-most limit of the thoracic cord.

Quantification of fluorescence in cortex to evaluate either AAV injection or shRNA electroporation areas was performed as previously described (Greig et al., 2016). Briefly, matched coronal $50 \mu\text{m}$ thick sections from Kihl14WT and Kihl14^{flox/flox} brains ($n = 4$ mice for each genotype), all with comparable AAV injections, were imaged for tdTomato on the injected side. Similarly, matched coronal sections from scrambled and Kihl14 shRNA electroporated brains ($n = 4$ mice for each group), all with comparable electroporations, were imaged for EGFP. In order to quantify fluorescence across the entire mediolateral extent of labeled cortical hemisphere, the straighten plug-in for ImageJ (Kocsis et al., 1991) was first used to straighten the cortical hemisphere. The resulting rectangular image was binned into 100 segments, using the divide slice function in Adobe Photoshop, and fluorescence intensity in each bin was quantified using the measure function in ImageJ. A plot of normalized average fluorescence intensity (and standard error of the mean) against mediolateral position across all brains was generated, and the difference between means for each group was analyzed using an unpaired Student's t test.

For all experiments, the person analyzing images was blinded to the experimental conditions.

QUANTIFICATION AND STATISTICAL ANALYSIS

Details of imaging quantification methodologies are described in Method Details. All n values and p values are also listed in figure legends. GraphPad Prism version 8 was used to perform statistical tests.

Data distributions were assumed to be normal, but this was not formally tested. For axon counts in Kihl14 shRNA experiments, as well for analysis of normalized CST fluorescence intensity quantification in Kihl14 conditional deletion experiments we used a two-sided t test. We used a two-way ANOVA with repeated-measures followed by Fisher's least significance difference posthoc test for the axon extension analyses in Crim1^{GCE} mice. For the comparison of three groups in Crim1^{GCE} mice, we used a one-way ANOVA followed by Tukey's honest significant difference (HSD) posthoc test. No statistical methods were used to pre-determine sample sizes. Variance between groups was analyzed using the f-test procedure.

Supplementary Material

Refer to Web version on PubMed Central for supplementary material.

ACKNOWLEDGMENTS

We thank Erica Gornstein, Ryan Richardson, Eva Gillis-Buck, Thomas Addison, Karen Wang, and Bonnie Wall for technical assistance; Macklis laboratory members for input; and Harvard Center for Biological Imaging for infrastructure support. Kihl14 mice were created from embryonic stem cell clone (EPD0735_1_H02) from KOMP Repository (<https://www.komp.org>), generated by the Wellcome Trust Sanger Institute. CSD targeted allele methods from Skarnes et al. (2011). Support comes from National Institutes of Health (NIH; R01s NS045523, NS075672; additional infrastructure by NS049553, NS104055, DP1NS106665), ALS Association, Travis Roy Foundation, and Massachusetts Department of Public Health to J.D.M. V.S. was partially supported by NIH (NTRAIN/NICHD K12HD093427) and DEARS Foundation. S.J.S. was partially supported by NIH predoctoral NRSA F31 NS063516. Y.I. had partial support by the Uehara Memorial Foundation, Kanae Foundation, Murata Overseas Scholarship Foundation, and DEARS Foundation. J.D.M. is an Allen Distinguished Investigator of the Paul G. Allen Frontiers Group.

REFERENCES

- Akintunde A, and Buxton DF (1992). Differential sites of origin and collateralization of corticospinal neurons in the rat: a multiple fluorescent retrograde tracer study. *Brain Res* 575, 86–92. [PubMed: 1504786]
- Arlotta P, Molyneaux BJ, Chen J, Inoue J, Kominami R, and Macklis JD (2005). Neuronal subtype-specific genes that control corticospinal motor neuron development in vivo. *Neuron* 45, 207–221. [PubMed: 15664173]
- Bruijn LI, Miller TM, and Cleveland DW (2004). Unraveling the mechanisms involved in motor neuron degeneration in ALS. *Annu. Rev. Neurosci* 27, 723–749. [PubMed: 15217349]
- Canty AJ, and Murphy M (2008). Molecular mechanisms of axon guidance in the developing corticospinal tract. *Prog. Neurobiol* 85, 214–235. [PubMed: 18378059]
- Cederquist GY, Azim E, Shnider SJ, Padmanabhan H, and Macklis JD (2013). Lmo4 establishes rostral motor cortex projection neuron subtype diversity. *J. Neurosci* 33, 6321–6332. [PubMed: 23575831]

- Charron F, and Tessier-Lavigne M (2005). Novel brain wiring functions for classical morphogens: a role as graded positional cues in axon guidance. *Development* 132, 2251–2262. [PubMed: 15857918]
- Chen B, Schaevitz LR, and McConnell SK (2005a). Fez1 regulates the differentiation and axon targeting of layer 5 subcortical projection neurons in cerebral cortex. *Proc. Natl. Acad. Sci. USA* 102, 17184–17189. [PubMed: 16284245]
- Chen JG, Rasin MR, Kwan KY, and Sestan N (2005b). Zfp312 is required for subcortical axonal projections and dendritic morphology of deep-layer pyramidal neurons of the cerebral cortex. *Proc. Natl. Acad. Sci. USA* 102, 17792–17797. [PubMed: 16314561]
- Chiu HS, York JP, Wilkinson L, Zhang P, Little MH, and Pennisi DJ (2012). Production of a mouse line with a conditional Crim1 mutant allele. *Genesis* 50, 711–716. [PubMed: 22511315]
- Dasen JS, Liu J-PP, and Jessell TM (2003). Motor neuron columnar fate imposed by sequential phases of Hox-c activity. *Nature* 425, 926–933. [PubMed: 14586461]
- Donoghue JP, and Wise SP (1982). The motor cortex of the rat: cytoarchitecture and microstimulation mapping. *J. Comp. Neurol* 212, 76–88. [PubMed: 6294151]
- Fame RM, MacDonald JL, and Macklis JD (2011). Development, specification, and diversity of callosal projection neurons. *Trends Neurosci* 34, 41–50. [PubMed: 21129791]
- Franco SJ, and Müller U (2013). Shaping our minds: stem and progenitor cell diversity in the mammalian neocortex. *Neuron* 77, 19–34. [PubMed: 23312513]
- Galazo MJ, Emsley JG, and Macklis JD (2016). Corticothalamic Projection Neuron Development beyond Subtype Specification: Fog2 and Intersectional Controls Regulate Intraclass Neuronal Diversity. *Neuron* 91, 90–106. [PubMed: 27321927]
- Ghosh A, Haiss F, Sydekum E, Schneider R, Gullo M, Wyss MT, Mueggler T, Baltés C, Rudin M, Weber B, and Schwab ME (2010). Rewiring of hindlimb corticospinal neurons after spinal cord injury. *Nat. Neurosci* 13, 97–104. [PubMed: 20010824]
- Greig LC, Woodworth MB, Galazo MJ, Padmanabhan H, and Macklis JD (2013). Molecular logic of neocortical projection neuron specification, development and diversity. *Nat. Rev. Neurosci* 14, 755–769. [PubMed: 24105342]
- Greig LC, Woodworth MB, Greppi C, and Macklis JD (2016). Ctip1 Controls Acquisition of Sensory Area Identity and Establishment of Sensory Input Fields in the Developing Neocortex. *Neuron* 90, 261–277. [PubMed: 27100196]
- Han W, Kwan KY, Shim S, Lam MM, Shin Y, Xu X, Zhu Y, Li M, and Sestan N (2011). TBR1 directly represses Fezf2 to control the laminar origin and development of the corticospinal tract. *Proc. Natl. Acad. Sci. USA* 108, 3041–3046. [PubMed: 21285371]
- Harding SD, Armit C, Armstrong J, Brennan J, Cheng Y, Haggarty B, Houghton D, Lloyd-MacGilp S, Pi X, Roochun Y, et al. (2011). The GUDMAP database—an online resource for genitourinary research. *Development* 138, 2845–2853. [PubMed: 21652655]
- Itoh Y, Sahni V, Shnyder SJ, and Macklis JD (2021). Lumican regulates cervical corticospinal axon collateralization via non-autonomous crosstalk between distinct corticospinal neuron subpopulations. *bioRxiv* 10.1101/2021.03.26.437104.
- James RE, and Broihier HT (2011). Crimpy inhibits the BMP homolog Gbb in motoneurons to enable proper growth control at the Drosophila neuromuscular junction. *Development* 138, 3273–3286. [PubMed: 21750037]
- Joshi PS, Molyneaux BJ, Feng L, Xie X, Macklis JD, and Gan L (2008). Bhlhb5 regulates the postmitotic acquisition of area identities in layers II–V of the developing neocortex. *Neuron* 60, 258–272. [PubMed: 18957218]
- Kamiyama T, Kameda H, Murabe N, Fukuda S, Yoshioka N, Mizukami H, Ozawa K, and Sakurai M (2015). Corticospinal tract development and spinal cord innervation differ between cervical and lumbar targets. *J. Neurosci* 35, 1181–1191. [PubMed: 25609632]
- Katz PS, and Harris-Warrick RM (1999). The evolution of neuronal circuits underlying species-specific behavior. *Curr. Opin. Neurobiol* 9, 628–633. [PubMed: 10508740]
- Kocsis E, Trus BL, Steer CJ, Bisher ME, and Steven AC (1991). Image averaging of flexible fibrous macromolecules: the clathrin triskelion has an elastic proximal segment. *J. Struct. Biol* 107, 6–14. [PubMed: 1817611]

- Kolle G, Georgas K, Holmes GP, Little MH, and Yamada T (2000). CRIM1, a novel gene encoding a cysteine-rich repeat protein, is developmentally regulated and implicated in vertebrate CNS development and organogenesis. *Mech. Dev* 90, 181–193. [PubMed: 10642437]
- Kwan KY, Lam MM, Krsnik Z, Kawasaki YI, Lefebvre V, and Sestan N (2008). SOX5 postmitotically regulates migration, postmigratory differentiation, and projections of subplate and deep-layer neocortical neurons. *Proc. Natl. Acad. Sci. USA* 105, 16021–16026. [PubMed: 18840685]
- Lai T, Jabaudon D, Molyneaux BJ, Azim E, Arlotta P, Menezes JR, and Macklis JD (2008). SOX5 controls the sequential generation of distinct corticofugal neuron subtypes. *Neuron* 57, 232–247. [PubMed: 18215621]
- Lemon RN (2008). Descending pathways in motor control. *Annu. Rev. Neurosci* 31, 195–218. [PubMed: 18558853]
- Lemon RN, and Griffiths J (2005). Comparing the function of the corticospinal system in different species: organizational differences for motor specialization? *Muscle Nerve* 32, 261–279. [PubMed: 15806550]
- Leone DP, Srinivasan K, Chen B, Alcamo E, and McConnell SK (2008). The determination of projection neuron identity in the developing cerebral cortex. *Curr. Opin. Neurobiol* 18, 28–35. [PubMed: 18508260]
- Li XG, Florence SL, and Kaas JH (1990). Areal distributions of cortical neurons projecting to different levels of the caudal brain stem and spinal cord in rats. *Somatosens. Mot. Res* 7, 315–335. [PubMed: 2248004]
- Liu Y, Shi J, Lu CC, Wang ZB, Lyuksyutova AI, Song XJ, and Zou Y (2005). Ryk-mediated Wnt repulsion regulates posterior-directed growth of corticospinal tract. *Nat. Neurosci* 8, 1151–1159. [PubMed: 16116452]
- Liu Y, Latremoliere A, Li X, Zhang Z, Chen M, Wang X, Fang C, Zhu J, Alexandre C, Gao Z, et al. (2018). Touch and tactile neuropathic pain sensitivity are set by corticospinal projections. *Nature* 561, 547–550. [PubMed: 30209395]
- Lodato S, Molyneaux BJ, Zuccaro E, Goff LA, Chen HH, Yuan W, Meleski A, Takahashi E, Mahony S, Rinn JL, et al. (2014). Gene co-regulation by Fezf2 selects neurotransmitter identity and connectivity of corticospinal neurons. *Nat. Neurosci* 17, 1046–1054. [PubMed: 24997765]
- Lodato S, Shetty AS, and Arlotta P (2015). Cerebral cortex assembly: generating and reprogramming projection neuron diversity. *Trends Neurosci* 38, 117–125. [PubMed: 25529141]
- Maguire CA, Bovenberg MS, Crommentuijn MH, Niers JM, Kerami M, Teng J, Sena-Esteves M, Badr CE, and Tannous BA (2013). Triple bioluminescence imaging for in vivo monitoring of cellular processes. *Mol. Ther. Nucleic Acids* 2, e99. [PubMed: 23778500]
- Martin JH (2005). The corticospinal system: from development to motor control. *Neuroscientist* 11, 161–173. [PubMed: 15746384]
- McKenna WL, Betancourt J, Larkin KA, Abrams B, Guo C, Rubenstein JL, and Chen B (2011). Tbr1 and Fezf2 regulate alternate corticofugal neuronal identities during neocortical development. *J. Neurosci* 31, 549–564. [PubMed: 21228164]
- Miller MW (1987). The origin of corticospinal projection neurons in rat. *Exp. Brain Res* 67, 339–351. [PubMed: 3622693]
- Molofsky AV, Kelley KW, Tsai H-HH, Redmond SA, Chang SM, Madireddy L, Chan JR, Baranzini SE, Ullian EM, and Rowitch DH (2014). Astrocyte-encoded positional cues maintain sensorimotor circuit integrity. *Nature* 509, 189–194. [PubMed: 24776795]
- Molyneaux BJ, Arlotta P, Hirata T, Hibi M, and Macklis JD (2005). Fezl1 is required for the birth and specification of corticospinal motor neurons. *Neuron* 47, 817–831. [PubMed: 16157277]
- Molyneaux BJ, Arlotta P, Menezes JR, and Macklis JD (2007). Neuronal subtype specification in the cerebral cortex. *Nat. Rev. Neurosci* 8, 427–437. [PubMed: 17514196]
- Neafsey EJ, Bold EL, Haas G, Hurley-Gius KM, Quirk G, Sievert CF, and Terberry RR (1986). The organization of the rat motor cortex: a microstimulation mapping study. *Brain Res* 396, 77–96. [PubMed: 3708387]
- Ozdinler PH, and Macklis JD (2006). IGF-I specifically enhances axon outgrowth of corticospinal motor neurons. *Nat. Neurosci* 9, 1371–1381. [PubMed: 17057708]

- Penfield W, and Boldrey E (1937). Somatic motor and sensory representation in the cerebral cortex of man as studied by electrical stimulation. *Brain* 60, 389–443.
- Penfield W, and Rasmussen T (1950). *The cerebral cortex of man. A clinical study of localization of function* (Macmillan)
- Pennisi DJ, Wilkinson L, Kolle G, Sohaskey ML, Gillinder K, Piper MJ, McAvoy JW, Lovicu FJ, and Little MH (2007). Crim1^{KST264/KST264} mice display a disruption of the Crim1 gene resulting in perinatal lethality with defects in multiple organ systems. *Dev. Dyn* 236, 502–511. [PubMed: 17106887]
- Raper J, and Mason C (2010). Cellular strategies of axonal pathfinding. *Cold Spring Harb. Perspect. Biol* 2, a001933. [PubMed: 20591992]
- Sahni V, Engmann A, Ozkan A, and Macklis JD (2020). Motor cortex connections. In *Neural Circuit and Cognitive Development, Second Edition*, Rubenstein J, Rakic P, Chen B, and Kwan KY, eds. (Academic Press), pp. 167–199.
- Sahni V, Shnyder SJ, Jabaudon D, Song JHT, Itoh Y, Greig LC., and Macklis JD (2021). Corticospinal neuron subpopulation-specific developmental genes prospectively indicate mature segmentally specific axon projection targeting. *Cell Rep* 37. 10.1016/j.celrep.2021.109843.
- Salie R, Niederkofler V, and Arber S (2005). Patterning molecules; multitasking in the nervous system. *Neuron* 45, 189–192. [PubMed: 15664170]
- Salinas S, Proukakis C, Crosby A, and Warner TT (2008). Hereditary spastic paraplegia: clinical features and pathogenetic mechanisms. *Lancet Neurol* 7, 1127–1138. [PubMed: 19007737]
- Serradj N, Paixão S, Sobocki T, Feinberg M, Klein R, Kullander K, and Martin JH (2014). EphA4-mediated ipsilateral corticospinal tract misprojections are necessary for bilateral voluntary movements but not bilateral stereotypic locomotion. *J. Neurosci* 34, 5211–5221. [PubMed: 24719100]
- Shim S, Kwan KY, Li M, Lefebvre V, and Sestan N (2012). Cis-regulatory control of corticospinal system development and evolution. *Nature* 486, 74–79. [PubMed: 22678282]
- Skarnes WC, Rosen B, West AP, Koutsourakis M, Bushell W, Iyer V, Mujica AO, Thomas M, Harrow J, Cox T, et al. (2011). A conditional knockout resource for the genome-wide study of mouse gene function. *Nature* 474, 337–342. [PubMed: 21677750]
- Starkey ML, Bleul C, Zörner B, Lindau NT, Mueggler T, Rudin M, and Schwab ME (2012). Back seat driving: hindlimb corticospinal neurons assume forelimb control following ischaemic stroke. *Brain* 135, 3265–3281. [PubMed: 23169918]
- Tennant KA, Adkins DL, Donlan NA, Asay AL, Thomas N, Kleim JA, and Jones TA (2011). The organization of the forelimb representation of the C57BL/6 mouse motor cortex as defined by intracortical microstimulation and cytoarchitecture. *Cereb. Cortex* 21, 865–876. [PubMed: 20739477]
- Tomassy GS, De Leonibus E, Jabaudon D, Lodato S, Alfano C, Mele A, Macklis JD, and Studer M (2010). Area-specific temporal control of corticospinal motor neuron differentiation by COUP-TFI. *Proc. Natl. Acad. Sci. USA* 107, 3576–3581. [PubMed: 20133588]
- Ueno M, Nakamura Y, Li J, Gu Z, Niehaus J, Maezawa M, Crone SA, Goulding M, Baccei ML, and Yoshida Y (2018). Corticospinal Circuits from the Sensory and Motor Cortices Differentially Regulate Skilled Movements through Distinct Spinal Interneurons. *Cell Rep* 23, 1286–1300.e7. [PubMed: 29719245]
- Ullan J, and Artieda J (1981). Somatotopy of the corticospinal neurons in the rat. *Neurosci. Lett* 21, 13–18. [PubMed: 7207864]
- Wang X, Liu Y, Li X, Zhang Z, Yang H, Zhang Y, Williams PR, Alwahab NSA, Kapur K, Yu B, et al. (2017). Deconstruction of Corticospinal Circuits for Goal-Directed Motor Skills. *Cell* 171, 440–455.e14. [PubMed: 28942925]
- Wang Z, Maunze B, Wang Y, Tsoulfas P, and Blackmore MG (2018). Global Connectivity and Function of Descending Spinal Input Revealed by 3D Microscopy and Retrograde Transduction. *J. Neurosci* 38, 10566–10581. [PubMed: 30341180]
- Welniarz Q, Dusart I, and Roze E (2017). The corticospinal tract: Evolution, development, and human disorders. *Dev. Neurobiol* 77, 810–829. [PubMed: 27706924]

- Wise SP, Murray EA, and Coulter JD (1979). Somatotopic organization of corticospinal and corticotrigeminal neurons in the rat. *Neuroscience* 4, 65–78. [PubMed: 759986]
- Woodworth MB, Greig LC, Kriegstein AR, and Macklis JD (2012). SnapShot: cortical development. *Cell* 151, 918–918.e1. [PubMed: 23141546]
- Woodworth MB, Greig LC, Liu KX, Ippolito GC, Tucker HO, and Macklis JD (2016). Ctip1 Regulates the Balance between Specification of Distinct Projection Neuron Subtypes in Deep Cortical Layers. *Cell Rep* 15, 999–1012. [PubMed: 27117402]
- Woolsey CN, Settlage PH, Meyer DR, Sencer W, Pinto Hamuy T, and Travis AM (1952). Patterns of localization in precentral and “supplementary” motor areas and their relation to the concept of a premotor area. *Res. Publ. Assoc. Res. Nerv. Ment. Dis* 30, 238–264. [PubMed: 12983675]
- Yao Z, Liu H, Xie F, Fischer S, Boeshaghi AS, Adkins RS, Aldridge AI, Ament SA, Pinto-Duarte A, Bartlett A, et al. (2020). An integrated transcriptomic and epigenomic atlas of mouse primary motor cortex cell types. *bioRxiv* 10.1101/2020.02.29.970558.
- Zhang Y, Fan J, Ho JW, Hu T, Kneeland SC, Fan X, Xi Q, Sellarole MA, de Vries WN, Lu W, et al. (2016). Crim1 regulates integrin signaling in murine lens development. *Development* 143, 356–366. [PubMed: 26681494]

Highlights

- Distinct molecules direct corticospinal neuron (CSN) axons to distinct spinal levels
- Crim1, a transmembrane protein, regulates thoracolumbar CSN axon extension
- Kelch-like 14 (Klhl14) regulates bulbar-cervical CSN axon extension
- This control occurs prior to axon collateralization, independent of axon connectivity

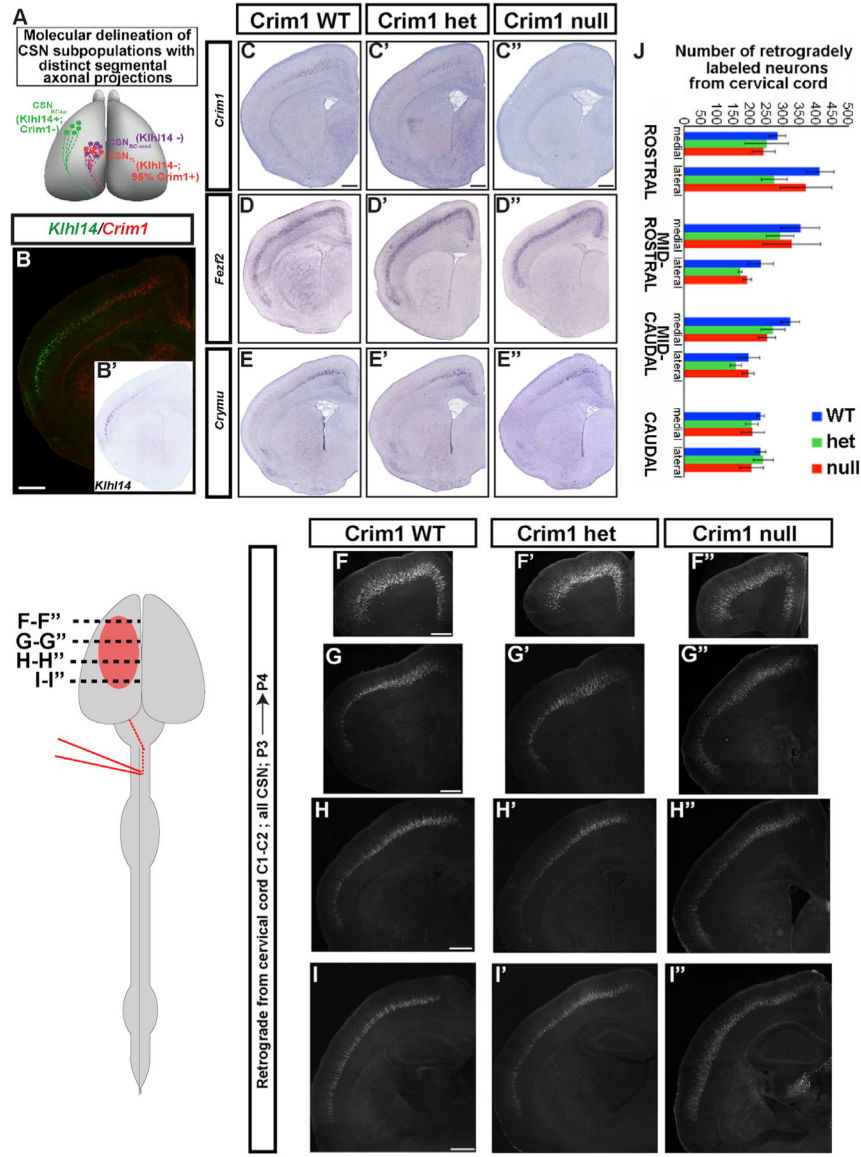


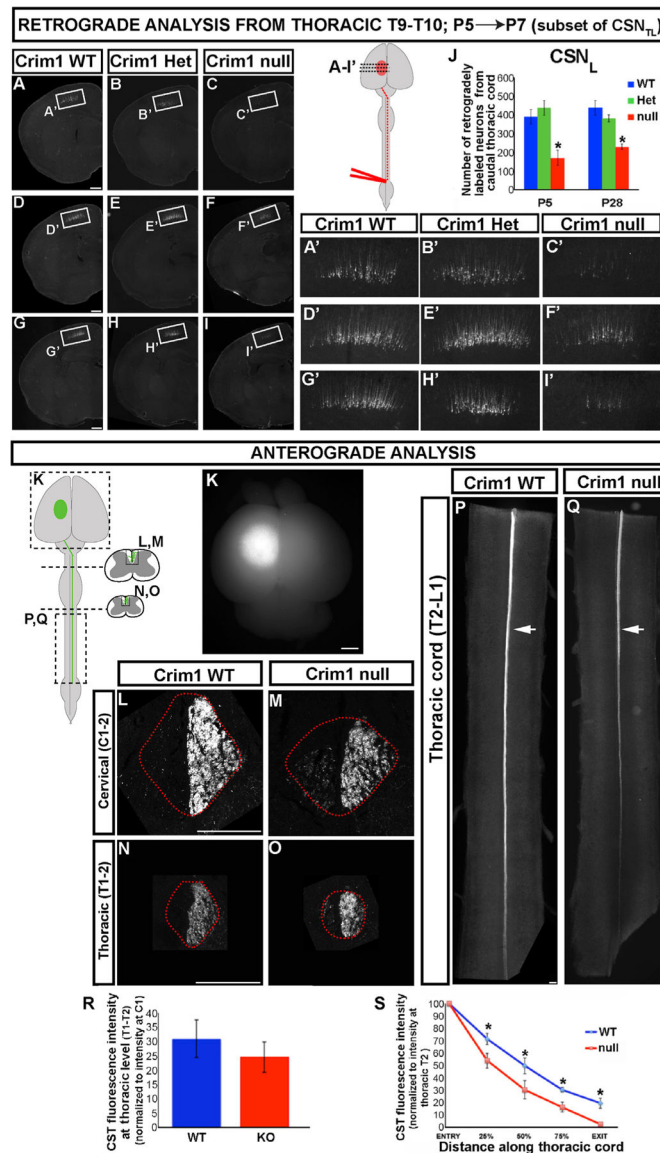
Figure 1. CSN are specified normally and project normally to the spinal cord in *Crim1*-null mice (A) Schematic outlining delineation of three segmentally specific CSN subpopulations (spatially distinct CSN_{BC-lat} and interdigitated CSN_{BC-med} and CSN_{TL}), indicating their molecular expression, axon extension, and axon collateralization, from the accompanying paper (Sahni et al., 2021). These CSN subpopulations are molecularly delineated during development and display persistent axon targeting before their final connectivity is established. *Kih14* expression delineates *Kih14*-positive CSN_{BC-lat} (green) from *Kih14*-negative CSN_{BC-med} (purple); all CSN_{TL} (red) are *Kih14* negative, and 95% ± 2% of CSN_{TL} express *Crim1* during early development. (B) Overlay of inverted and pseudocolored *in situ* hybridization images from the accompanying paper (Sahni et al., 2021) showing complementary expression of *Kih14* (green) and *Crim1* (red) in cortex. The inset (B') shows *Kih14* is restricted to CSN_{BC-lat} in lateral cortex.

(C–E'') *In situ* hybridization from P4 *Crim1* WT, heterozygous, and homozygous mice. Homozygotes are null for *Crim1* expression (C–C'') but exhibit normal *Fezf2* (D''); all CSN) and *Cry-mu* (E''); CSN_{medial}) expression.

(F–I'') Coronal sections of P4 brains retrogradely labeled from C1 at P3. *Crim1* nulls have normal CSN distribution.

(J) Quantification of numbers of CSN retrogradely labeled from C1 in *Crim1* WT, heterozygous, and null mice. There is no difference between groups.

Scale bars: 500 μ m.



(L–O) Axial views of the dorsal funiculi in Crim1 WT (L and N) and Crim1 nulls (M and O) at C1-C2 (L and M) and T1-T2 (N and O). Red dotted lines indicate dorsal funiculus. There is no visual difference between groups.

(P and Q) Composite image created by overlaying a series of horizontal sections of the thoracic cord from WT (P) and Crim1 nulls (Q). WT CSN_{TL} axons extend through thoracic cord to its caudal-most limit, reaching lumbar cord. While a significant number of Crim1-null axons enter the thoracic cord, the majority of them fail to extend substantially caudally, and very few axons reach caudal thoracic levels. CST intensity drops substantially by only a quarter of the distance into the thoracic cord in Crim1 nulls (arrows).

(R) Quantification of fluorescence intensity of labeled CST axons in dorsal funiculus at T1-T2 normalized to intensity at C1-C2. There is no significant difference between groups.

(S) Quantification of fluorescence intensity of labeled CST axons in dorsal funiculus of horizontal sections of the thoracic cord at specific distances (from rostral to caudal) in WT and Crim1 nulls. CST axon intensity significantly decreases by 25% of the distance into the thoracic cord in Crim1 nulls ($p = 0.0125$ by two-way ANOVA with repeated measures, $*p < 0.05$ by Fishers LSD).

Scale bars: (A–I) 500 μm ; (K) 1 mm; (L–Q) 100 μm .

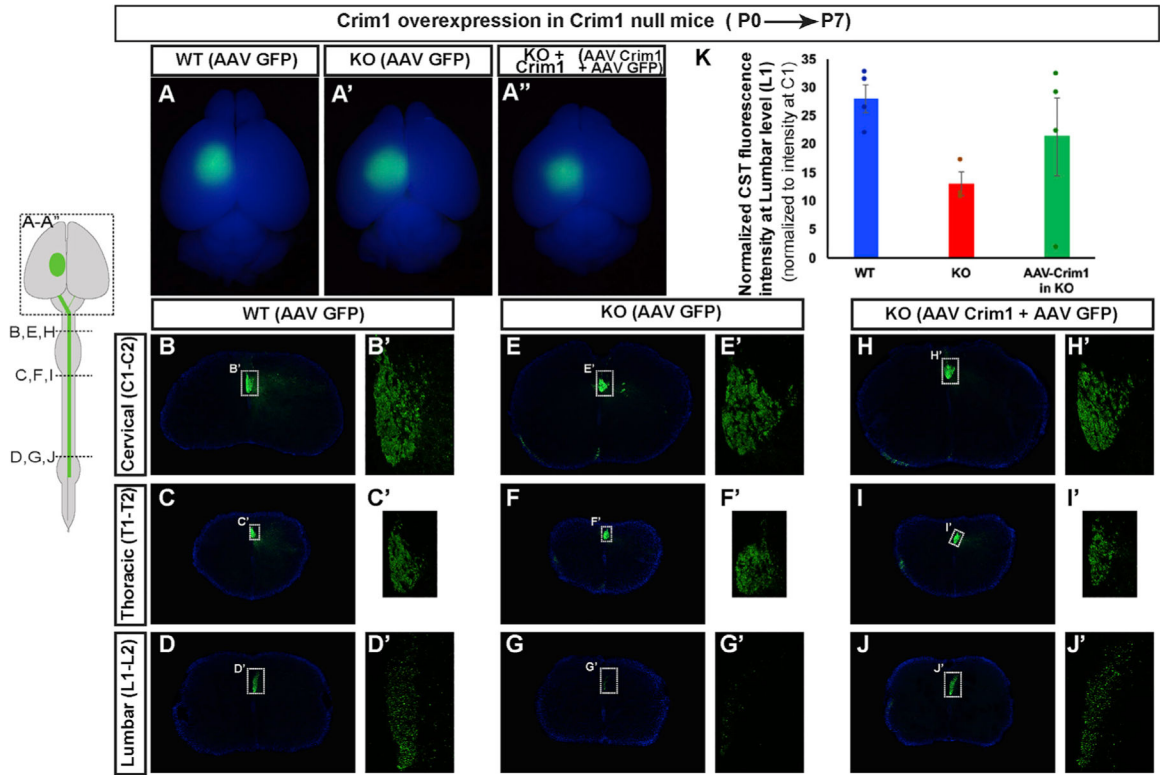


Figure 3. Crim1 functions predominantly cell autonomously in CSN_{TL} to enable axon extension to thoracolumbar segments

(A–A'') Whole-mount images of P7 brains from WT (A) and Crim1 nulls (KO) (A') injected in medial cortex at P0 with AAV engineered to express EGFP (AAV-EGFP). (A'') Whole-mount image of a P7 Crim1-null brain co-injected at P0 with AAV2/1 engineered to overexpress Crim1 (AAV-Crim1) along with AAV-EGFP (KO + Crim1).

(B–J') Axial spinal sections from the same P7 mice at cervical (B, E, and H), thoracic (C, F, and I), and lumbar (D, G, and J) segments. There is no difference in CSN axon extension from C1-C2 to T1-T2 among all three groups. In striking contrast, there is a substantial reduction in the number of CSN axons that reach L1-L2 in KO mice compared to WT controls (D and D' versus G and G') or KO + Crim1 mice (J and J'). This indicates “rescue” by cortical expression of Crim1.

(K) Quantification of fluorescence intensity of labeled CST axons in dorsal funiculus at L1-L2 normalized to intensity at C1-C2. KO mice have very substantially (>50%) reduced CST intensity compared to WT mice ($p = 0.005$ by Student's *t* test). There is no difference in CST intensity between WT and KO + Crim1 (“rescue”) mice.

Scale bars: (A–A'') 1 mm; (B–J) 100 μ m.

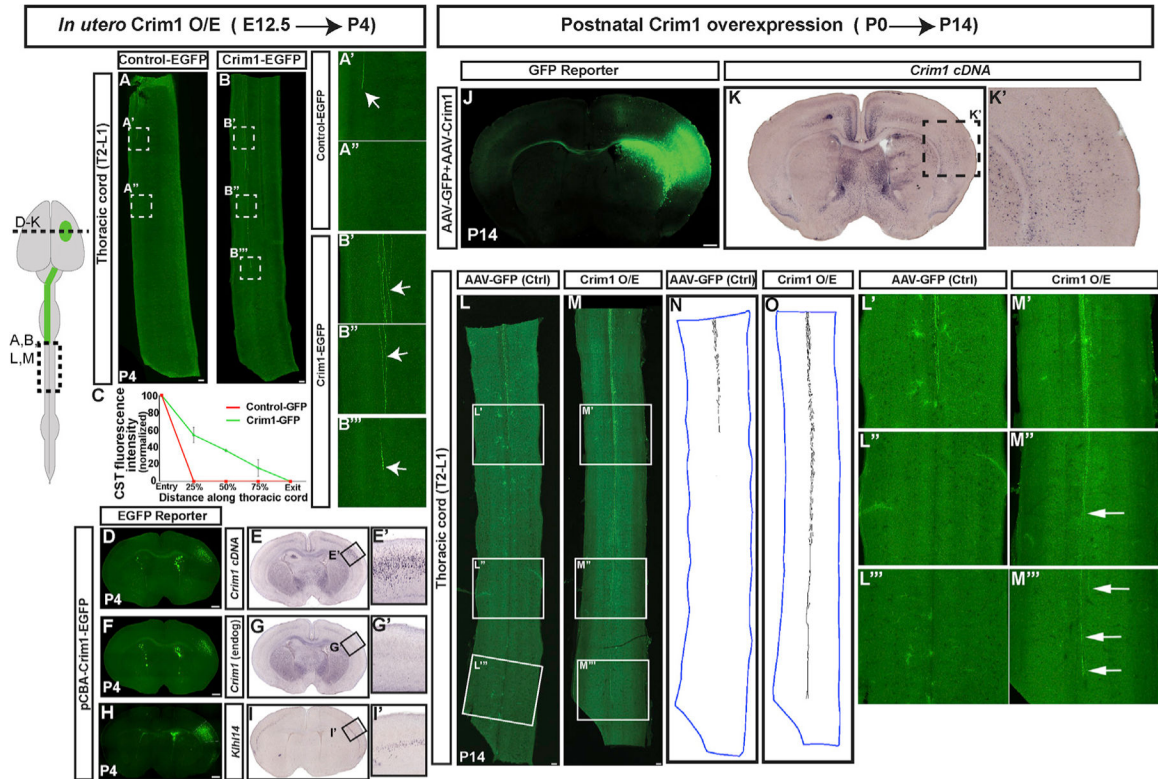


Figure 4. Crim1 is sufficient to redirect CSN_{BC-lat} axons past cervical cord to caudal spinal segments

In (A)–(I), plasmids, designed to overexpress EGFP alone (control-EGFP) or Crim1 and EGFP (Crim1-EGFP), were delivered to developing CSN_{BC-lat} in lateral cortex using *in utero* electroporation at E12.5, with tissue collected at P4 for analysis.

(A–B''') Assembled composite images created by overlaying a series of sagittal thoracic cord sections from control-EGFP (A) and Crim1-EGFP (B) electroporated mice. The few CSN_{BC-lat} axons entering thoracic cord in control mice terminate within the first few thoracic segments and do not reach farther than 25% of the distance into thoracic cord (A' and A''). Crim1-EGFP-expressing CSN_{BC-lat} axons extend significantly farther (arrows in B' and B'') with a few individual axons extending as far as 75% of the distance into thoracic cord (arrows in B''').

(C) Quantification of fluorescence intensity of EGFP+ axons in either control EGFP or Crim1-EGFP electroporated mice at four sites along the rostro-caudal extent of the thoracic cord. Each data point represents average normalized intensity ± SEM (n = 3 mice per group; p = 0.0002 by two-way ANOVA with repeated measures, *p < 0.001 by Fishers LSD test).

(D–I') Coronal sections of a single P4 brain electroporated *in utero* at E12.5 with Crim1-EGFP. (D, F, and H) EGFP fluorescence (green) shows electroporated area in lateral cortex. (E) *In situ* hybridization for *Crim1* cDNA showing *Crim1* overexpression on the electroporated side (magnified in E'). *Crim1* is normally restricted to medial cortex, and there is no upregulation of endogenous *Crim1* in Crim1-overexpressing CSN_{BC-lat} (G, magnified in G'). Also, *Khl14* expression in Crim1-overexpressing CSN_{BC-lat} remains unchanged (I, I').

(J–M''') AAV-Crim1 co-injected with AAV-EGFP (reporter) into rostralateral cortex at P0. AAV-EGFP alone is the control. Tissue was collected at P14. (J–K') Coronal section of a brain injected with AAV-EGFP+AAV-Crim1 showing injection site in rostralateral cortex (J). *In situ* hybridization for Crim1 cDNA shows overexpressed *Crim1* in injection site (K, magnified in K'). (L–M''') Assembled composite images created by overlaying a series of thoracic cord horizontal sections from control (L) and AAV-EGFP + AAV-Crim1 (M) (Crim1O/E) injected mice. Labeled axons in Crim1 O/E mice extend substantial distances into thoracic cord (magnified images in M'–M'''), with few axons reaching the caudal-most levels of thoracic cord (arrows in M'' and M''').

(N and O) Inverted, high-contrast monochrome tracings from (L) and (M) of EGFP+ axons. Blue outlines the cord, and black pixels show EGFP+ axons (details in STAR Methods). Scale bars: (A, B, L, and M) 100 μm ; (D–K) 500 μm .

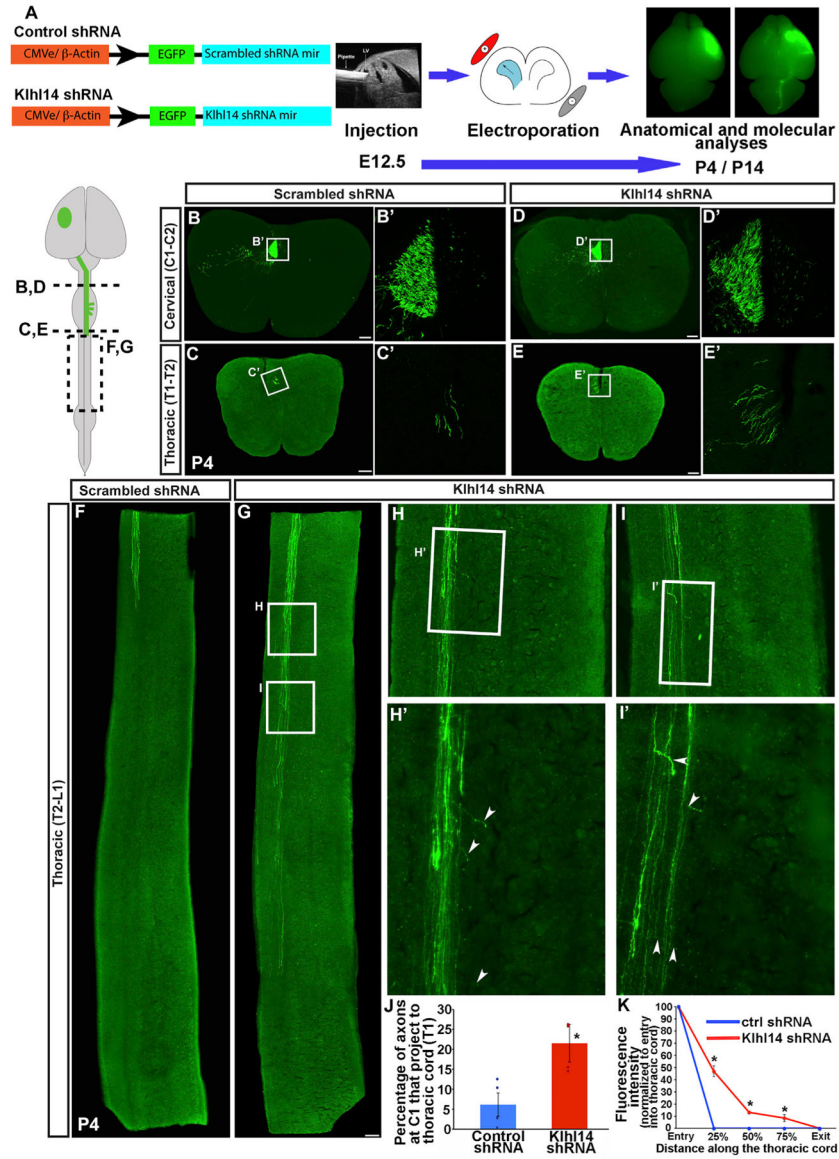


Figure 5. Reduction in Kihl14 function causes aberrant targeting of CSN_{BC}-lat axons beyond the cervical cord

(A) Plasmids designed to express either control scrambled shRNA or a shRNA to knock down Kihl14 expression. shRNA sequences were placed 3' to an EGFP coding sequence. The constructs were electroporated into lateral cortex at E12.5, and tissue is collected at P4 and P14 for analysis (electroporated brains in Figure S3). Images shown are immunocytochemistry for EGFP on axial (B–E) or sagittal (F and G) sections of the cord. (B–E) Axial sections at cervical C1–C2 (B and D) and thoracic T1–T2 (C and E) from mice that were electroporated with scrambled (B and C) or Kihl14 shRNA (D and E). (B'–E') High-magnification single-plane confocal images of the dorsal funiculus (areas boxed in B–E). (F and G) Assembled composite images created by overlaying a series of sagittal sections of thoracic cord from scrambled (F) and Kihl14 shRNA (G) electroporated mice. Kihl14-

(F and G) Assembled composite images created by overlaying a series of sagittal sections of thoracic cord from scrambled (F) and Kihl14 shRNA (G) electroporated mice. Kihl14-

shRNA-expressing CSN_{BC-lat} axons extend significantly farther into thoracic cord (arrows in G).

(H-I') Magnified views of boxed regions in (G) showing Klh14-shRNA-expressing CSN_{BC-lat} axons aberrantly extending collaterals in thoracic cord (arrowheads H' and I').

(J) Quantification of percentage of axons in the dorsal funiculus at C1-C2 that extend to T1-T2. Graphs represent average percentages \pm SEM (n = 4 mice for each group [control and Klh14 shRNA]; *p < 0.05 by Student's t test).

(K) Quantification of normalized fluorescence intensity of labeled EGFP+ axons in the dorsal funiculus on all sagittal sections of thoracic cord from either control scrambled-shRNA- or Klh14-shRNA-electroporated mice. Each data point represents the average normalized intensity \pm SEM (p < 0.0001 by two-way ANOVA with repeated measures; *p < 0.001 by Fishers LSD test).

Scale bars: 100 μ m.

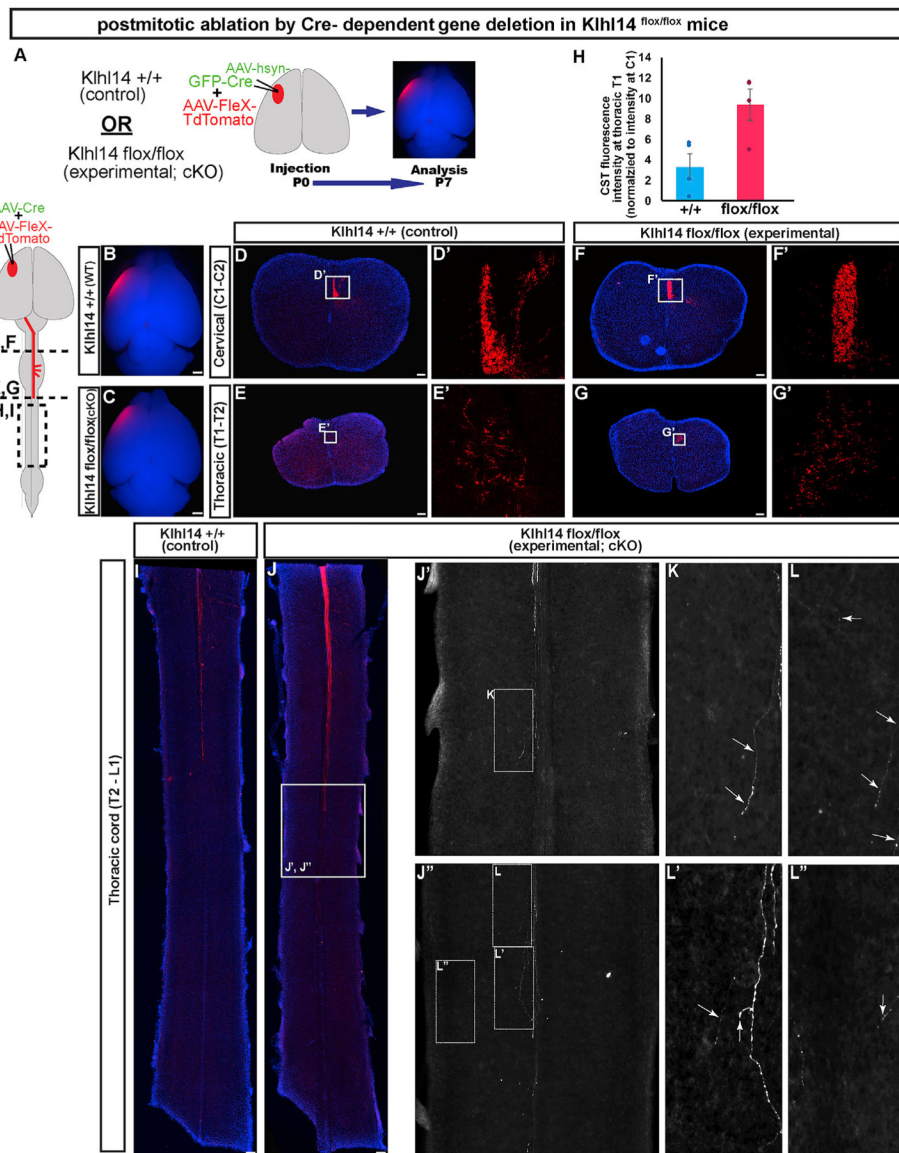


Figure 6. *Klhl14* functions in postmitotic CSN_{BC-lat} early postnatally, specifically when CSN axons are extending into cervical cord

(A) AAV-Cre and AAV-FLEX-tdTomato were co-injected into rostralateral cortex at P0 in *Klhl14* WT control or *Klhl14*^{fllox/fllox} mice to conditionally ablate *Klhl14* function in CSN_{BC-lat} (*Klhl14* cKO). Mice were perfused at P7, and axons were visualized using immunocytochemistry for tdTomato.

(B and C) Whole-mount images of P7 brains from *Klhl14* WT and *Klhl14* cKO mice that were injected with AAV-Cre + AAV-FLEX-tdTomato at P0. tdTomato fluorescence (red) demarcates closely matching injection site and extent in all mice (quantification in Figure S5).

(D–G'). Axial sections at cervical C1-C2 (D and F) and thoracic T1-T2 (E and G) from either WT (D and E) or *Klhl14* cKO mice (F and G). (D'–G') High-magnification single-plane confocal images of the dorsal funiculus (areas boxed in D–G). Substantially more axons extend to T1-T2 in *Klhl14* cKO mice compared to controls.

(H) Quantification of fluorescence intensity of tdTomato+ CSN_{BC-lat} axons at T1-T2 normalized to C1-C2 in Klhl14 WT versus Klhl14 cKO mice. Graphs show average percentages \pm SEM (n = 4 mice for each group [WT and Klhl14 cKO]; *p < 0.05 by Student's t test).

(I–J'') Assembled composite images created by overlaying a series of horizontal sections of thoracic cord from either Klhl14 WT (I) or Klhl14 cKO (J) mice showing strikingly extended, aberrant CSN_{BC-lat} projections in thoracic cord. (J' and J'') Monochrome, magnified views of boxed region in (J) at two separate Z levels, showing aberrant gray matter collaterals at these caudal thoracic levels in Klhl14 cKO mice.

(K–L'') Higher magnification views of boxed regions in (J') and (J'') showing these collaterals (arrowheads K and L–L'').

Scale bars: (B and C) 1 mm; (D–G, I, and J) 100 μ m.

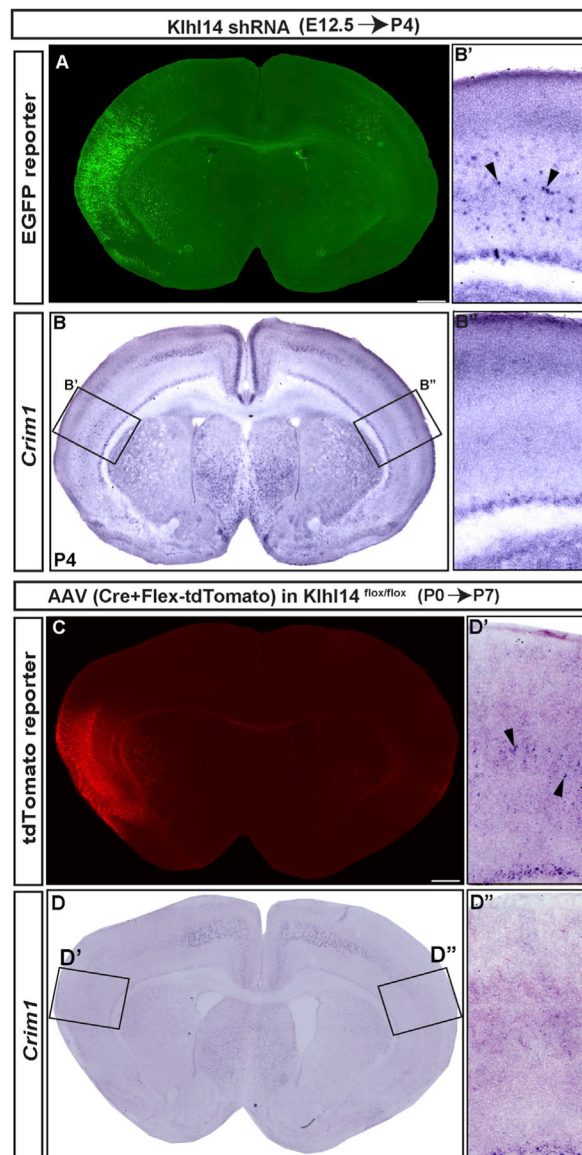


Figure 7. Reduction or deletion of Kihl14 function causes ectopic *Crim1* expression in lateral cortex

(A–B'') Coronal section of a P4 brain electroporated *in utero* at E12.5 with Kihl14 shRNA. (A) EGFP fluorescence (green) shows electroporation in lateral cortex. (B) *In situ* hybridization on the same section showing *Crim1* expression. *Crim1* is normally restricted to medial cortex. However, Kihl14 shRNA causes ectopic *Crim1* expression (arrowheads) in lateral cortex (B'), only in electroporated hemisphere (compare B' and contralateral B''). (C–D'') Coronal section of a P7 Kihl14 cKO brain injected with AAV-Cre + AAV-FLEX-tdTomato at P0. (C) TdTomato fluorescence (red) shows injection in lateral cortex. (D) *In situ* hybridization on the same section showing *Crim1* expression. Similar to Kihl14 shRNA, postmitotic Cre-dependent Kihl14 deletion causes ectopic *Crim1* expression (arrowheads) in lateral cortex (D'), only in injected hemisphere (compare D' and contralateral D''). Scale bars: 500 μ m.

KEY RESOURCES TABLE

REAGENT or RESOURCE	SOURCE	IDENTIFIER
Antibodies		
Rabbit anti-CTIP2	Abcam	Cat# ab28448; RRID:AB_1140055
Rabbit anti-Fog2	Santa Cruz Biotechnology	Cat# sc-10755; RRID:AB_2218978
Mouse anti-SATB2	Abcam	Cat# ab51502; RRID:AB_882455
Rabbit anti-GFP	Molecular Probes	Cat# A-1112; RRID:AB_221569
Chicken anti-GFP	Thermo Fisher Scientific	Cat# A10262; RRID:AB_2534023
Rabbit anti-RFP	Rockland	Cat# 600-401-379; RRID:AB_2209751
Bacterial and virus strains		
AAV-8 hsyn-GFP-Cre	UNC vector core	N/A
AAV-2/1 FleX-TdTomato	University of Pennsylvania (now at Addgene)	N/A
AAV2/1 CAG-Crim1	This paper	N/A
AAV2/1 CAG-Klh14	This paper	N/A
AAV2/1 CAG-EGFP	vector core at Massachusetts General Hospital, Boston, MA	Maguire et al., 2013
Chemicals, peptides, and recombinant proteins		
Cholera Toxin B subunit, Alexa 555 conjugate	ThermoFisher	Cat # C34776
Critical commercial assays		
Dual-Luciferase Reporter 1000 Assay system	Promega	Cat # E1980
Experimental models: Organisms/strains		
Crim1 ^{GCE} mice	(mice obtained from Jackson laboratories) Stock number: 017495	GUDMAP database (Harding et al.; 2011)
Klh14 flox mice	Embryonic stem cell clones obtained from KOMP database; mice generated in this paper	Skarnes et al., 2011
Oligonucleotides		
See Table S1 for oligonucleotide information		N/A
Recombinant DNA		
pCAG-GFP-T2A-Klh14	This paper	N/A
pCAG-Crim1	This paper	N/A
pGIPZ-Klh14 -shRNAmir clones	Open Biosystems	N/A
Software and algorithms		
ImageJ	NIH	https://imagej.nih.gov/ij/
GraphPad Prism 8.0	GraphPad	https://www.graphpad.com/scientific-software/prism/